POLITECNICO DI TORINO

Master's Degree in Mechatronic Engineering

Master's Degree Thesis

Bio-Inspired Fin-Based 3D Maneuvering For Underwater Robots

Supervisors

Prof. Alessandro RIZZO

Prof. Claudio ROSSI

Candidate

Giambattista CARUSO

February 2023

Abstract

In the field of robot development, nowadays, bio-inspired solutions are on the ascendancy. This is due to many reasons, but we can mainly summarise them through the ideal of pursuing an engineering 'leitmotif': *improving performance and overcome current technologies*. In fact, if we look at living organisms as autonomous systems, they are, without any doubt, the most sophisticated robust and adaptable systems we know. The living beings we see every day are the result of millions of years of evolution, they have achieved a very high level of adaptation to their environment, and often their solutions to survive (in terms of body structure or behaviour) are the most efficient imaginable [**8**]. So, it is immediate to think about a kind of reverse engineering applied to the animal world to understand and exploit its characteristics in order to find new, alternative and efficient solutions for modern challenges. All those branches of engineering concerned with developing new technologies on the basis of biodiversity observation can be framed in this light. Obviously, in the world of underwater robotics, the main source of inspiration are fishes. To date, however, there are many problems that slow down the development of this field, mainly related to the limitations of current materials and technologies and to the difficulties associated with the underwater environment.

The aim of this work is therefore to realise a complete model of a fish-inspired robot, without traditional actuators, controlled by means of innovative fins that use SMA wires to generate motion. Specifically, the objective is to assess the magnitude of the torques generated by the fins' movements and to test the feasibility of a control strategy based on the superposition of the individual measured effects.

The document is structured with a first chapter in which an exhaustive state of the art on bio-inspired robotics is presented. Then, in the second and third chapter, the technical features related to the design and realisation of the model and the experiments are explained. Finally, the fourth chapter shows and comments on the results obtained.

Acknowledgements

Un sentito ringraziamento a tutti i professori ed in particolare ai miei relatori, i prof. A. Rizzo e C. Rossi, i vostri insegnamenti sono stati e saranno sempre di ispirazione per il mio lavoro.

Un grazie speciale alla mia famiglia, che mi ha sempre supportato (e sopportato) durante questi anni e soprattutto non ha mai smesso farmi sentire il proprio affetto.

A mia madre Pina e mio padre Giovanni, per aver sempre creduto in me, incondizionatamente.

A mia sorella Maria, per essere sempre stata una fonte di ispirazione.

A mia nonna Gasperina e ai suoi innumerevoli rosari.

A tutti i miei amici che, nonostante fossi sempre a centinaia di chilometri dalla mia Lamezia, mi hanno sempre fatto sentire a casa.

A todos los españoles que me han apoyado durante el último año y medio, os prometo que nos vamos a ver pronto.

Grazie per aver reso questo percorso il migliore che potessi desiderare.

Table of Contents

List of Tables

List of Figures

Introduction

In this work, a realistic model of robotic fish was realised. It has a rigid body made of ABS and flexible fins made of silicone. The model designed allows the fins to move individually or jointly and is obviously submersible. In particular, shape-memory alloys, which perform a function similar to that of the muscle fibres, were used to perform movements, replacing traditional motors.

This document has been structured to firstly give an overview of the current state of technology and research in the field of bio-inspired robotics. As the state of the art will show, in fact, the field of bio-robotics is very broad and includes a very wide range of different implementations. The aim is therefore to contextualise the proposed work within one of its most innovative branches, which is the one of the bio-inspired underwater robotics implemented using unconventional materials.

Subsequently, in the document, a detailed description of all the designed and manufactured components is given, with particular attention to the materials and methods.

Finally, the results are presented; they are categorised according to the various fins and movements performed, so that a clear picture of the measurements taken can be obtained.

In addition, there are two appendices: appendix A is intended to clarify some fundamental aspects implied in the document, while appendix B provides information on the realised planning and the possible implications of this kind of robots.

General objective

The general objective of this work is to assess the feasibility of underwater 3D maneuvering realised through fins controlled without the use of motors.

The reason why it was decided to carry out this type of study is that, to date, there is not a great deal of scientific analysis on the 3D manoeuvring involving complete models of fish-inspired underwater robots. Usually, in fact, fins tend to be analysed individually and this, therefore, leads to partial results about the manoeuvring.

Specific objectives

The specific objectives are:

- fins construction;
- design and construction of the body , the support and the connection system;
- design and construction of the electronic circuits needed;
- development of the necessary codes;
- realisation of an HMI for a real-time use of the sensor;
- design and practical integration of the experiment platform;
- design and realisation of the experiments;
- data analysis.

Chapter 1

State of the Art of Bio-Inspired Robotics

When it comes to robotics inspired to the living world it is important to define properly the topic. We can identify four different branches:

- Bio-morphism → develop robots that mimic the appearance of animals;
- Bio-inspired → use of biological characteristics in living organisms as the knowledge base for developing new robot designs;
- Bio-mimetic → develop robots that borrow their structure and senses from animals, such as humans or insects;
- Bio-mimicry → the design and production of materials, structures, and systems that are modelled on biological entities and processes.

Each of these categories deals in a different way with the same concept, and the same objective: *the development of bio-robotics.*

This chapter will mainly deal with the world of bio-inspired robotics, even if often the distinction between the categories presented above is not trivial.

1.1 Some examples of bio-inspired robotics

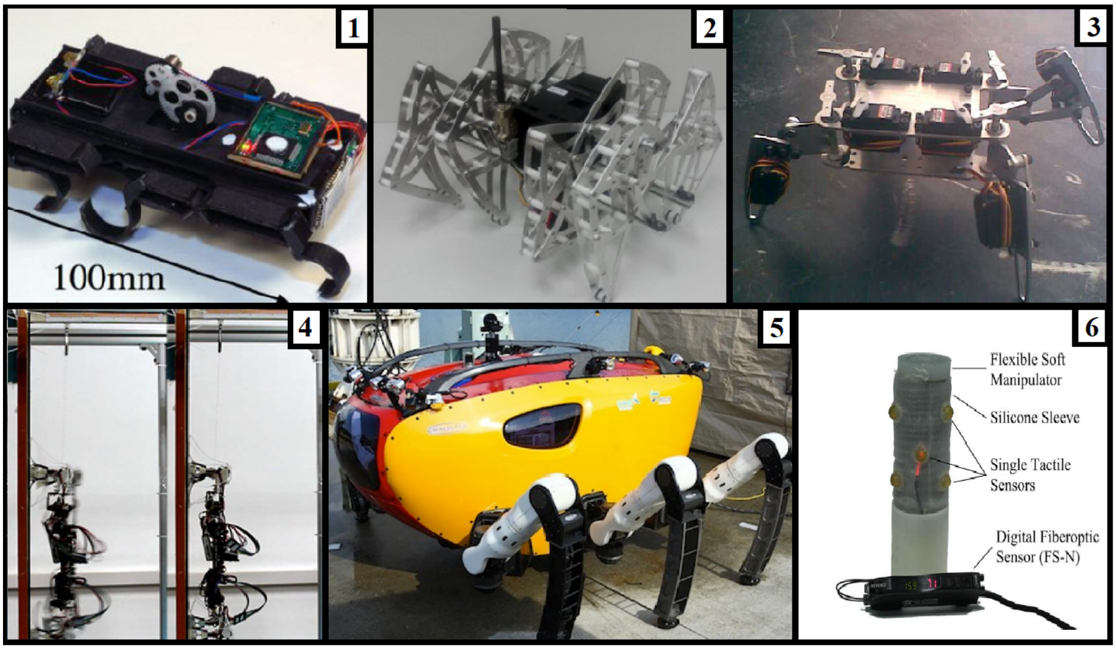

Figure 1.1: Some examples of bio-inspired robots. Images taken from [**1**, **2**, **3**, **4**, **6**, **9**]

The development of bio-inspired robotic systems started in the second half of the 20th century. Although, in the literature, it is possible to find references to automatic bio-inspired systems produced a few centuries earlier [**7**], but which have nothing to do with the modern canons of the discipline. Banally, the motivation is linked to the very high level of technology required to develop this type of systems, which obviously could not be achieved until a few decades ago. Indeed bio-inspired robotics is advancing rapidly not only for the extensive studies made by robotics researchers and the increasing investments from industries and governments worldwide, but also thanks to the advancement of sensing, actuation, and information technology achieved in the last years. Nowadays different robots or robotic systems inspired by animals, insects, and fish have already been developed [**7**, **8**]. The main brake on the development of bio-inspired robotics is that as far as the best technologies are available, there are no actuators that are as sophisticated as muscles, materials that are as soft as tissues, or joints that generate the complicated yet smooth motion that human and animal joints perform [**7**]. It is from this perspective that the importance of bio-inspired robotics can be seen. Clearly the development of robots that are similar to animals in mechanical and behavioural terms is not just an exercise in style, it is a way of developing new technologies that can address problems that seem unsolvable today, in a totally different way. Obviously, the topic is very broad; there are numerous examples of bio-inspired robots completely different from each other. In an attempt, therefore, to give a general idea of the current state of the art but maintaining a synthetic style, a few examples have been selected. The six robots showed in figure 1.1 were chosen on the basis of the variety of: applications, technologies, size and relevance of the publications. With regard to robots inspired precisely by fishes, there is a specific discussion of the topic in the section 1.3. Below are described the main features of the selected models; the circled number in the title of each subsection corresponds to the numbered labels in figure 1.1.

Bio-inspired design of a min-imally actuated six-legged robot 1

This robot is inspired by rapidly running arthropods, many other prototypes are inspired by these animals, such as: Sprawlita, iSprawl, Mini-Whegs etc.

This is due to the fact that arthropods can move very fast in relation to their size, they have a good ability to change their trajectory during motion and they are also energy-efficient [**2**].

Moreover, small size enables this kind of robots to operate in environments where large robots would be impractical and they have a low production cost.

The major challenge in building a small-scale light-weight many-legged robot is the minimization of the number of actuators required to produce effective locomotion. The prototype that they presented in the paper is actuated by a single DC motor and can reach the maximum speed of 1.4 m/s (14 body lengths/s) [**2**].

A key feature of this robot is the system that allows it to make curves. The robot turns by stiffening the middle leg on the opposite side of the desired turn direction. Currently, the stiffness of the leg varies depending on the material, but is very interesting the future goal of implementing a variable stiffness system based on shape memory alloy wires attached to the legs [**2**].

Bio-inspired robot platform powered by a PEM fuel cel 2

This is a good example of the potential of bio-inspired robotics, as it attempts to solve two fairly common problems with mobile robots:

- wheeled robot necessity of a smooth surface to travel;
- limitation due to the conventional batteries.

As we can see from the image, the robot is inspired by the locomotion system used by spiders. The development of the robot platform was designed considering the fuel cell system integration constraints and this is the key feature of this model.

The fuel cell system is more than 50% efficiency at maximum power, and the robot is able to operate up to 600 minutes in its most favourable configuration [**4**].

Miniature crab-like mobile robot ③

This robot is based on tetrapod locomotion because it has demonstrated to be the simplest legged-based locomotion ensuring the characteristics of omnidirectional motion, terrain adaption, and both static and dynamic stability.

This prototype exhibits interesting features such as compactness, lightweight, low implementation cost, low power consumption, and the capability of moving on irregular terrain at interesting speeds. Its controller enables both tele-operated and pre-programmed operation of the prototype, it has 32 min autonomy (operating at maximum speed) [**1**]. It has a low cost, about 250 USD and the eight servomotors actuating the tetrapod's 8-DOF provide a stable motion and develop a maximum speed of 0.076 m/s. Another interesting thing is that only one micro-controller is used to govern the motion of all four legs, which allows to simplify the control design avoiding the synchronization and multiplexing between several micro-controllers [**1**].

Gecko Robot with Bio-inspired Dry Adhesive Foot ④

This prototype was developed and oriented to on-orbit service. The gecko robot has 16 active degrees of freedom and 12 passive degrees of freedom, it can realize barrier-free movement in three-dimensional space, and it can achieve stable adhesive movement on the surface of the space station [**3**].

The main challenge faced by the researchers was to design a novel bionic adhesive gecko foot with large normal force, because in reality the gecko's climbing ability depends on the intermolecular forces between its countless setae on its toes and the surface of the object, known as Van Der Waals forces, and this kind of inner working is difficult to recreate. To achieve this goal they used dry adhesive materials in order to realize the gecko toes, while the whole foot is composed by four toes connected by a spherical joint and springs [**3**].

The Crabster CR200 ⑤

The CR200 is also inspired by crabs like the third robot described, but as we can see, the result is totally different. It is precisely for this reason that this model is included in this analysis, with the aim of highlighting how the possible solutions are infinite even though they are inspired by the same animals. This is a robot designed to perform underwater walking and manipulating in the presence of the strong tidal currents.

In fact, robotic underwater vehicles play an important role in marine research, environmental operations, deepwater exploration, and search-and-rescue missions [**6**]. The Crabster can remain on the sea floor for days at a time if necessary, as it is tethered to an external power source. It's equipped with a high resolution scanning sonar, acoustic camera, acoustic doppler current profiler (ADCP), and several optical cameras, it weighs about 600 kilos and its dimensions are 2.42x2.45x2 meters[**5**].

Tests carried out on this model have been satisfactory and have shown that it can be a viable alternative to the screw-driven vehicles [**6**].

Bio-Inspired Tactile Sensor Sleeve for Surgical Soft Manipulators 6

This is a completely different example than the previous ones, here, in fact, is presented a membrane for Robot-assisted Minimally Invasive Surgery (RMIS) that is not inspired by an animal feature but by a plant one, specifically it is inspired by cucumber tendrils. This is a new approach because so far, inspiration for surgical tools has been taken from snakes and octopuses [**9**]. Through this research, sensory elements, based on optic fibres, were developed. They are capable of measuring pressure, and if mounted on a soft surface they can provide haptic feedback to the surgeon without adding big limitation on the robot movements. Sensory elements were developed with two different materials (Ecoflex Supersoft silicone and Poly PT Flex rubber) highlighting that the stiffness of the tactile sensor material affects the measurable force range. Another key feature is that this device is MR-compatible (MR stands for Magnetic Resonance) [**9**]. The results are promising, although the influence of the membrane on the kinematics of the robot will need to be evaluated in the future and further miniaturisation is needed.

1.2 Analysis of academic interest related to the topic

In this section we will assess, through the number of publications pertaining to bio-inspired robotics, the interest regarding this branch of engineering. Due to the functioning of the search engines, in order to obtain the results that are presented in the continuation of the document, in the research were used the words "bio-inspired", "bioinspired" and "robotics". Moreover to avoid errors due to unconsolidated information, data up to 2020 were only considered.

The research was carried out on the main search engines: IEEE Xplore and Scopus. The aim is to assess the trend of this topic, from a general point of view and within the field of robotics. In particular are analysed the number of publications per year about the topic of "bio-inspired robotics" and the percentage of these publications compared to the total number of publications about "robotics". In this way it is possible to obtain information on the trend of this technology and in particular if it is in a phase of:

- growth → research
- stabilisation → application
- degrowth → phase of overcoming

Furthermore, the interest in this field can be seen by assessing the increase in the number of publications in each year. However, it is always important to not neglect the fact that values in absolute terms can be influenced by specific events and therefore they cannot be evaluated as unique metric.

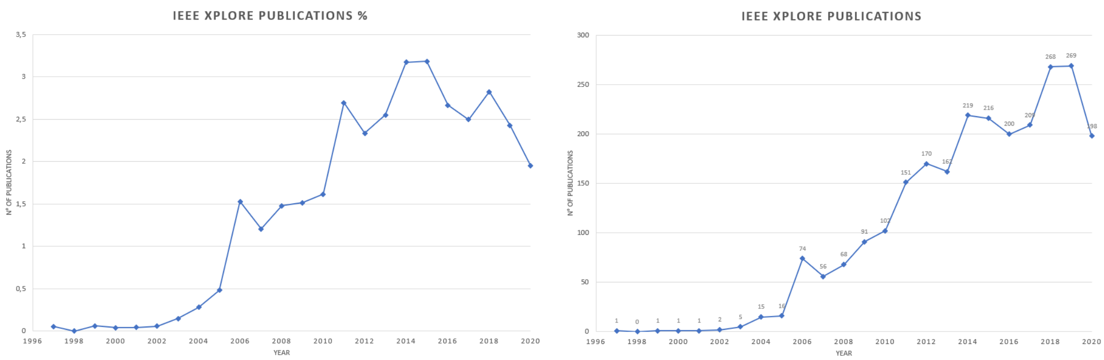

Figure 1.2: Number of publications per year as a percentage of the total and in absolutes terms in the IEEE database

On the basis of these graphs, globally, the trend can be described as one of growth, since, as can be seen, there is basically a steady increase in the number of publications over the years. However, if we look more deeply into the matter, we can see that in the last years there has been a decline. This behaviour could be due to countless factors, and in order to make most accurate considerations it is necessary to wait a few years so that we can actually see how the curve will evolve. However, on the basis of the distinction made earlier, we can say that the most likely hypothesis is that we are in the phase between research and application.

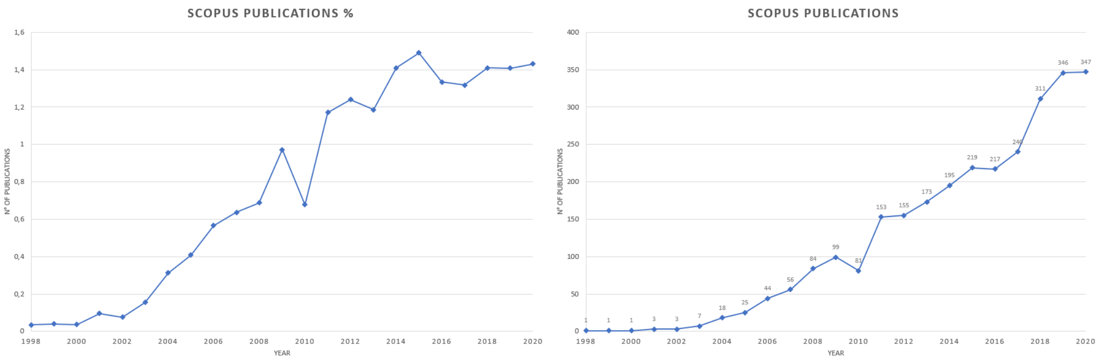

Figure 1.3: Number of publications per year as a percentage of the total and in absolutes terms in the Scopus database

The graphs obtained through Scopus are quite intuitive and describe a growing technology in both percentage and absolute terms, but that has been settling in recent years. In this case, we do not see the decrease phenomenon highlighted in the IEEE database.

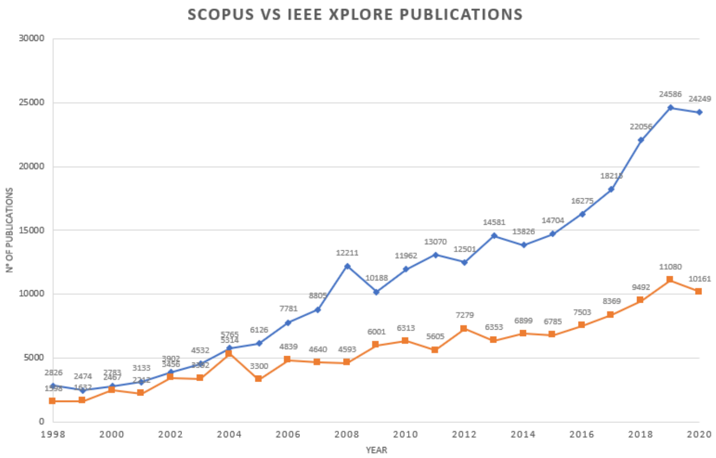

Figure 1.4: Number of publications per year in the Scopus and IEEE Xplore databases about the "robotics" topic. *Scopus data is shown in blue while the IEEE Xplore one is shown in orange*

Figure 1.4 shows the trends in terms of absolute publications in the two databases (about the “robotics" topic), in order to highlight how, actually, the numbers are related to the database analysed, but, overall, the trends are similar.

1.2.1 Considerations

With regard to the analysis of publications, we can see that the general trend in bio-inspired robotics is basically growing. In fact, the decreasing trend related to the IEEE Xplore database is probably due to some factor not related to the global tendency of the technology, actually, this kind of trend is not confirmed by Scopus. It can therefore be said that the research carried out has highlighted the interest on bio-inspired robotics and the substantial growth that this field is experiencing.

1.3 Focus on fish-inspired robots

As one of the most successful taxonomical groupings in the world, fishes occupy most of the water areas on earth. Their extraordinary swimming ability has attracted the interest of scholars for thousands of years [**10**] .

But due to the intractability of living creatures, and in particular of fishes, it's really difficult to conduct experiments on their biomechanics. For this reason, a fairly common approach is to recreate robotic models to approximate the characteristics of fishes and thus be able to investigate the desired phenomena on them. Moreover, in this way, it is possible to isolate individual movements and thus highlight the effects of each action individually. Of course, there is the problem of the degree of accuracy and reliability of the model, so that deriving the characteristics of living organisms from robotic models can still be risky and lead to false conclusions.

Anyway, this methodology remains to date among the most effective for the study of fish biomechanics, and, moreover, the aim of many studies is just to conceptually demonstrate that it is possible to artificially recreate systems that exploit the same movement strategies as fishes. Indeed, most of the fish-inspired robots want to solve the problem of the limitations of underwater robots with screw propulsion. The traditional approach is to create fish-like structures through complex mechanisms (generally with an high number of joints) that are driven by conventional motors and thus have poor performance and high noise levels. But, more recently, smart-materials (SMA, IPMC, piezoceramics etc.) have started to be used to try to overcome these limitations.

The main researches about the topic will be proposed and commented on in the following paragraphs.

1.3.1 Fins

Most researches based on fish biomechanics focuses on the study of fins [**10**, **11**, **12**, **14**, **18**]. The main approaches are two:

1 analyse fins separately and mount them on structures that serve simply for the purpose of performing the experiments;

2 build robots that have fish-like structures and carry out more realistic tests.

Anyway the main challenges remain the techniques of fins construction and fins control, usually, as we can see for example in the research of James Tangorra et al. [**14**] the structures of the fins are very complex and consequently their control is not trivial.

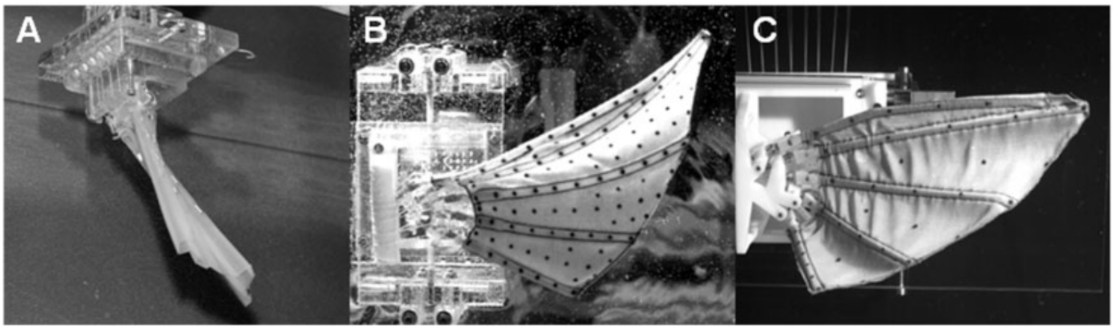

Figure 1.5: Example of bio-inspired fins. Image taken from [**14**]

This complexity derives from the fact that a peculiar characteristic of fishes is that they can change the shape of their fins surfaces thanks to three dimensions movements, thus making their construction or even numerical modelling quite complex. Simple rigid oscillating structures with the profile of a real fin can give results in terms of propulsion [**15**], but are still useless for manoeuvring. Therefore, when it comes to generate forces in order to allow the control of roll, pitch and yaw, it is necessary to construct mechanisms that allow movements in three dimensions such as those proposed in figure 1.5.

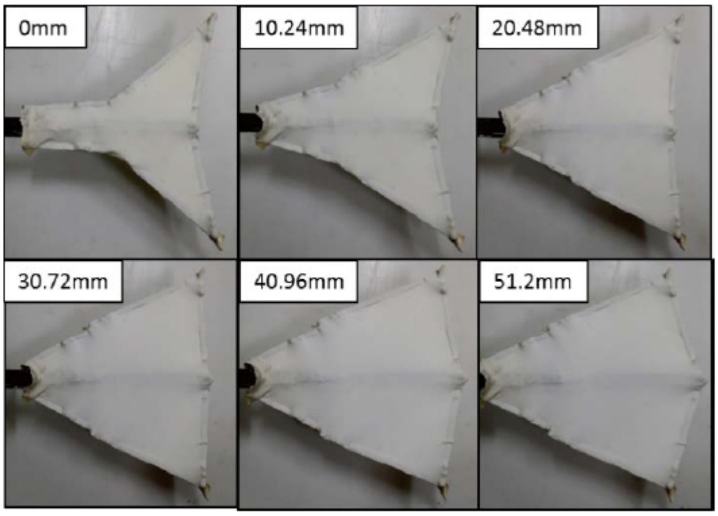

Figure 1.6: Example of a bio-inspired fin that can change its shape. The visible numbers are referred to the position of the rod that parameterises the shape of the fin. Image taken from [**12**]

However, innovative materials such as SMAs can be used to achieve this kind of result without the use of complex mechanical structures.

SMA

Shape memory alloys (SMAs) have been receiving increasingly more attention and study since the discovery and first publication of the shape memory effect by Chang and Read in 1951 [**17**]. These materials are characterized by two effects: the shape memory effect (SME) and the pseudoelastic effect, basically the most interesting characteristic of these materials is that they can return to their original shape after a deformation (even up to deformations in the order of 10% [**17**]) by rising up their temperature (SME effect). For further discussions, reference can be made to L. C. Brinson's paper [**17**] in which an exhaustive research about the SMAs has been made.

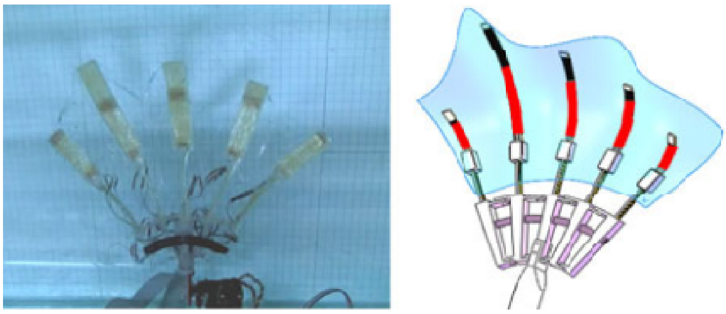

Figure 1.7: Example of a bio-inspired SMA-actuated fin: on the right is visible the design while on the left the real implementation. Image taken from [**22**]

Key parameters

Many studies carried out [**11**, **13**, **14**, **18**] have not only shown that it is possible to generate forces that could theoretically be able to move and control submarine robots through the use of bio-inspired fins, but have also demonstrated the possibility of modulating these forces according to various parameters. In general, regardless of the type of control and construction, the two main parameters highlighted are the angle at which the fin bends and the speed of the movement. Another parameter that can be influential depending on the strategies used for the control and construction of the fin is the rigidity of the fin itself. Unfortunately, the correlations between these parameters and the results in terms of magnitude of the forces generated are not trivial; an increase in the bending angle and the speed does not always correspond to an increase in the force generated. Furthermore, the correlation between the motion generated and the direction of the forces produced is quite complex. These peculiarities are due to the fact that the forces are generated by the complex interaction between fins and water, which is not a static agent because it is characterised by flows.

1.3.2 Pitch control by Centroid Adjustment

There are also 'hybrid' solutions for manoeuvring, in particular for pitch control there are prototypes that do not rely on the movement of fins to generate the necessary forces but on the movement of mechanisms within the submarine robot. As can be seen in the study proposed by W. Shao and C. Xu" [**15**], excellent results can be obtained by moving a weight within the fish structure. This kind of solutions allow the robot's centre of gravity to be modified and so to generate a rotation in pitch axis. Furthermore, as demonstrated in their research, this rotation can be controlled and stabilised by means of a simple PID controller.

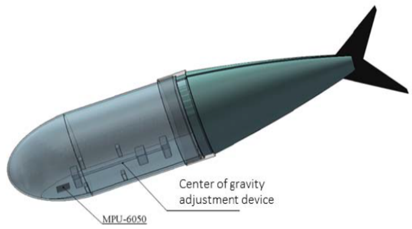

Figure 1.8: Solution proposed by W. Shao and C. Xu for pitch control. Image taken from [**15**]

1.3.3 Body

Studies concerning fish body are mainly focused on propulsion rather than manoeuvring [**20**]. In fact, depending on the species considered, body movement may be more or less influential in the animal's dynamics, but in general, when present, its primary purpose is propulsion. We can find traces of an early bio-inspired robot model made for the study of fish motion, already in 1993. It was realized by the MIT and it is known as Robot Tuna. It was followed later by a model capable of moving without supports called Robot Pike. Unfortunately, no more detailed information is available, but through the MIT portal it emerges that different versions of the two projects were developed.

As in fins case, the main problems are due to the complexity of the necessary mechanisms, but, thanks to innovative materials, are being made attempts in order to overcome these limitations [**19**]. The most interesting results are related to studies that correlate fins movements with body movement. In particular, some of these works, such as the study by Ziyu Ren et al. [**10**], highlight the phase difference between the movement of the tail and that of the caudal fin as a parameter that actively contributes to the fish manoeuvrability. This research has indeed shown that the forces generated by the caudal fin can be modified by varying this parameter (phase difference). Although, as expressed in the document [**10**], the relation between this factor and the generated forces requires further investigation.

Figure 1.9: Solution proposed by William Coral et al. Image taken from [**19**]

In figure 1.9 we can see another example of a robot realised for the study of body dynamics, in this case the actuation is performed by means of SMA wires and it has been demonstrated how its control can be effectively realised by means of simple PID systems. Anyway the aim of this work is to analyse fins manoeuvring so the body of the robot realised is not free to move. For this reason, even though there is a great deal of research on fish bodies, this topic was not further deepened.

1.3.4 Possible applications

As already commented, beyond the academic works aimed at studying the biomechanics of fishes, the main purpose of fish-inspired robots construction and development is to allow performing tasks that are impossible to do with traditional instruments or to improve the performance of the possible ones. A fish-like robot has become increasingly essential in marine exploration, underwater rescue, water quality monitoring, and other disciplines in recent years, thanks to rapid advancements in manufacturing, control, sensing, and other technologies [**13**]. For example, in figure 1.10 , taken from the review made by Prabhat K.V. et al. [**13**], we can see a prototype designed for dynamically monitoring the dissolved-oxygen level in aquafarms.

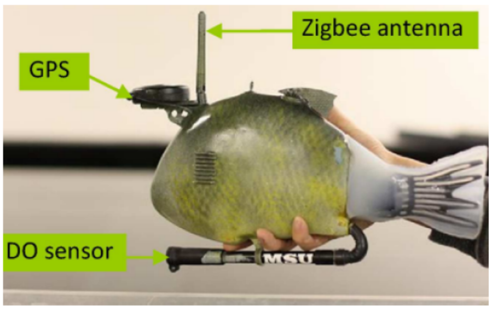

Figure 1.10: Prototype designed for dynamically monitoring the dissolved-oxygen level in aquafarms. Image taken from [**13**]

Chapter 2

Fish mechanical design and electronics

The body and the designed fins are inspired by those of a largemouth bass, a carnivorous fish in the centrarchidae (sunfish) family. They were sized based on a specimen of approximately 50 cm in length, a common adult. Refer to the appendix A for further details.

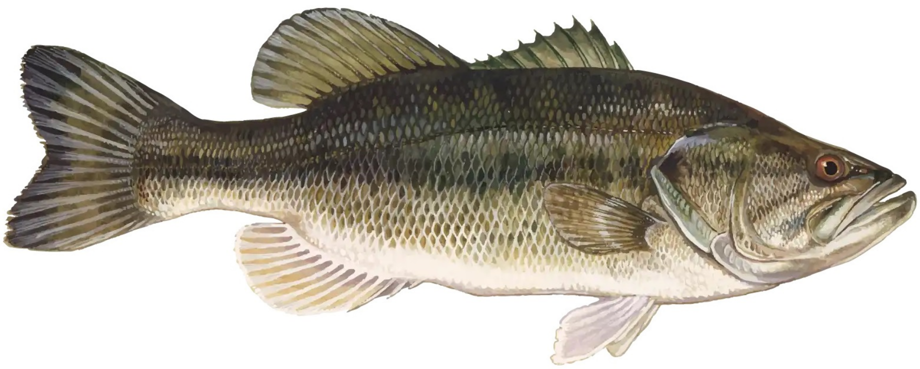

Figure 2.1: A largemouth bass (micropterus salmoides).

2.1 Fins design and construction

The realised fins are made of silicone inside which are arranged SMA wires that allow bending in two opposite directions. The direction in which the fin bends depends only on the positioning of the SMA wires inside the silicone. The fins are 3 millimetres thick and the SMA wires are placed 0.5 millimetres far from the middle of the fin on both sides. In this way, for example, the contraction of the SMA wire placed on the right side will cause the fin to bend to the right, and the contraction of the one placed on the left side to bend to the left.

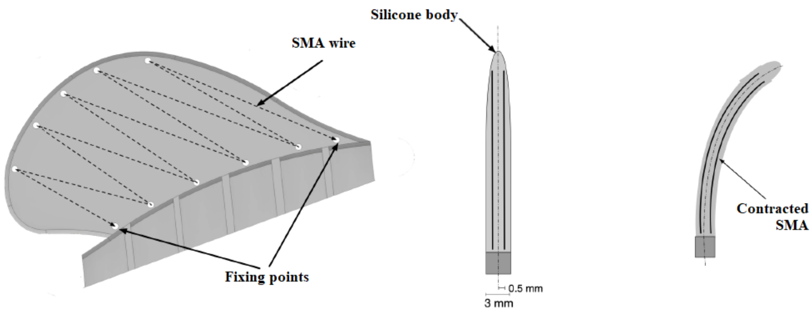

Figure 2.2: SMA-based fin [**21**].

The first step in the fin-making process was to design the moulds. CAD models of the fins were made from real images of the fish. Thank to this models the CADs of the moulds required for silicone injection were finally obtained. The moulds were subsequently produced by 3D printing. Each mould has two parts so that the fin removal and the SMA wires placement are feasible.

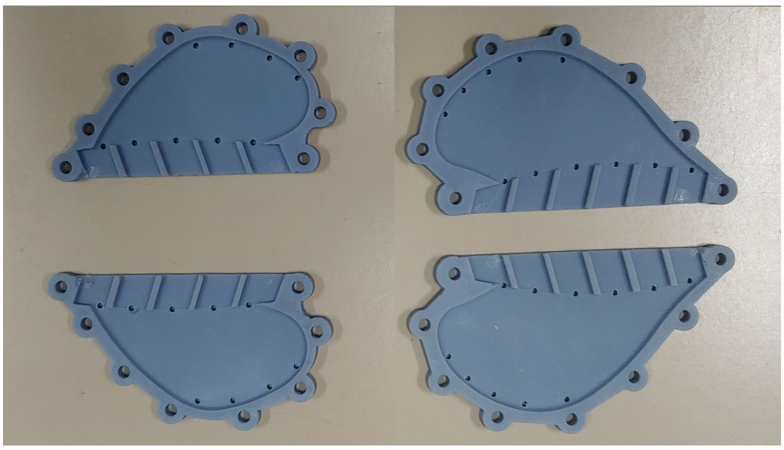

Figure 2.3: Moulds of the dorsal and anal fins.

In each half of the moulds there are 4-mm-diameter holes to allow the two parts to be connected by screws and 1.5-mm-diameter holes to allow the brackets to be inserted.

Brackets are specially designed supports, also 3D printed, which allow the SMA wires to be placed 0.5 mm far from the middle of the fins.

Figure 2.4: Bracket realized to support SMA wires.

The geometry with which the holes for the brackets were placed is based on the positioning of the fin rays of the real fish. Depending on the number of rays in each real fin, the number of folds of the SMA wire were planned such that a similar structure was obtained.

The material of which the fins are made is PlatSil Gel 25, a two-component platinum silicone, while the SMA wires selected are NiTi alloys from Flexinol, the following table shows the main characteristics of this material.

Type	Flexinol LT
Diameter	150 µm
Activation Temp	70°C
Resistance	55 Ω/m
Recommended Current	410 mA
Rec. Pull Force	321 grams
Rec. Deformation	3-5%

Table 2.1: SMA wires characteristics.

In order to be able to generate the current flow within the SMA wires and control them, each end of the SMA wires is connected to stranded wires of 0.07mm diameter. The connection was made using normal crimp ferrules.

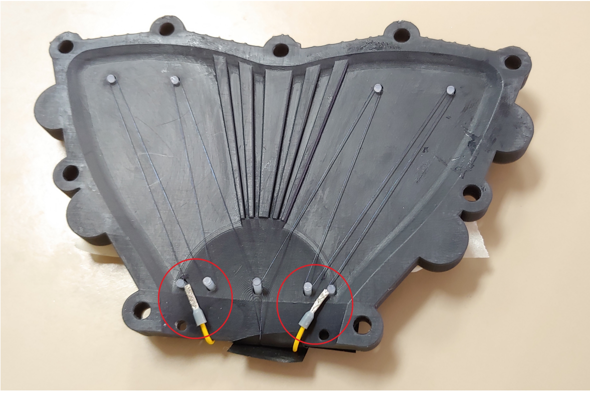

Figure 2.5: Mould of the caudal fin. The crimp ferrules connecting the wires used for the current supply and the SMA wires are highlighted.

Finally, below is presented the list with the necessary steps to make a fin:

1 insertion of brackets into moulds;

2 placement of the SMA wires;

3 connection through crimp ferrules of the supply wires and the SMA ones;

3.5 insertion of the rigid base for the connection between fin and fish (caudal fin only);

4 joining of the two mould halves;

5 silicone injection;

6 fin extraction.

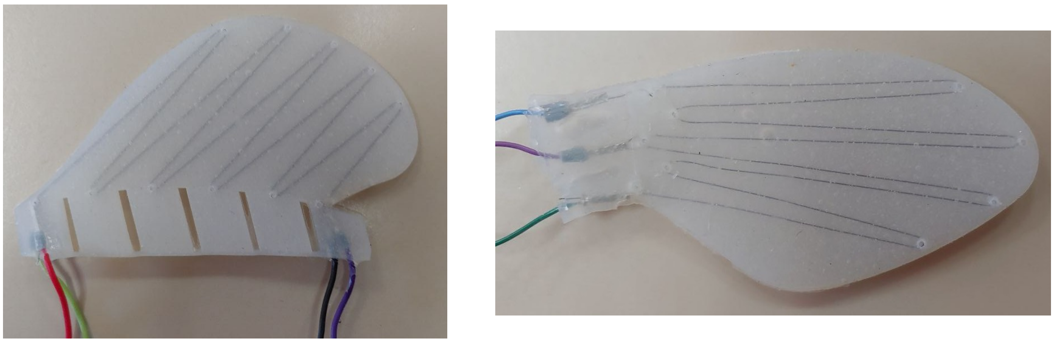

Figure 2.6: Examples of the realized fins. On the left is shown the dorsal fin while on the right the pectoral one.

2.1.1 Caudal fin features

The caudal fin, differently from the other fins, requires a slightly more complex manufacturing process. In fact, it has a base, also obtained by 3D printing, designed to allow a firm connection to the body of the fish and, furthermore, it is made using four SMA wires so that a greater variety of movements can be achieved. In fact in addition to the movements of the entire fin the upper or lower half can be controlled independently.

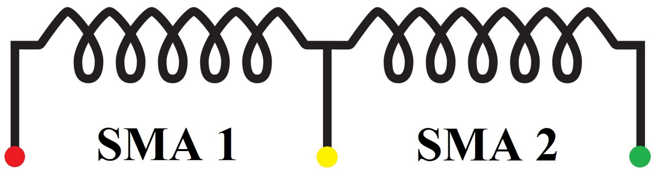

Figure 2.7: SMA wires connection in the caudal fin.

In figure 2.7 we can see the connection strategy used for the two SMA wires on each side of the caudal fin. Thanks to this connection, in fact, powering the red point and the yellow point produces the movement of the SMA wire 1, while powering the yellow point and the green point produces the movement of the SMA wire 2. Finally, by powering the red point and the green point, it is possible to obtain the simultaneous movement of the SMA wires 1 and 2. This feature allows precisely to control the whole fin or independently the upper and lower parts.

Figure 2.8: The caudal fin realised. Coloured dots have been marked with the same convention used previously, the dots are positioned at the points where the SMA wires are actually connected in order to make comprehension clearer. The rigid base can also be recognised in black.

2.2 Body design

The body of the model was made of ABS by 3D printing, the thickness of the model is 2 mm. The body was divided into two parts, the “trunk" and the head so that working inside the model could be possible during assembly. Furthermore, another advantage of the division is that the parts can be printed vertically with a minimal use of supports.

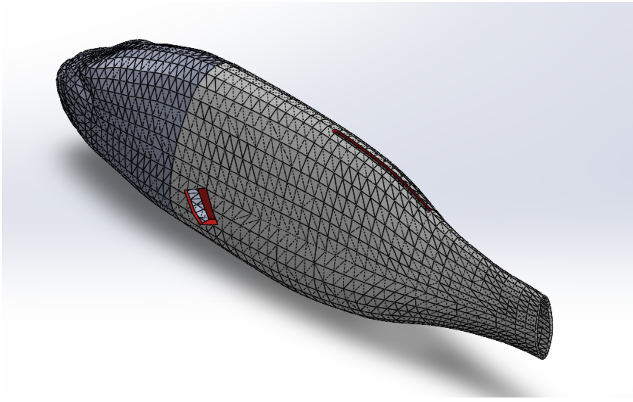

Figure 2.9: Isometric view showing the entire body of the fish designed. The two parts are highlighted with different colours.

In order to be able to connect the two parts, two cross-shaped supports were designed. The one connected at the base of the head has pivots while the one connected at the base of the body has corresponding holes. This makes possible to join or separate the two parts easily and without the need of adhesives.

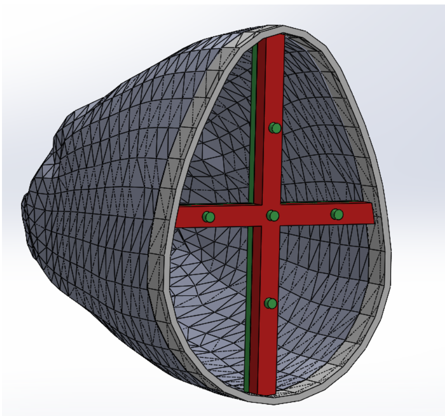

Figure 2.10: Cross-sectional view. The cross-shaped supports are highlighted with different colours.

To allow a proper fixing of the pectoral fins, supports inside the body shape were also designed. The decision to fit them inside depended on the fact that external supports would have damaged the fluid dynamics of the model.

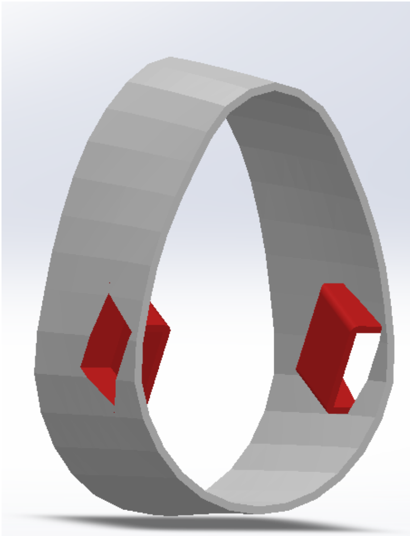

Figure 2.11: Cross-sectional view showing the supports designed to allow the fixing of the pectoral fins

To allow the dorsal fin and anal fin connection, slotted holes were made at the attachment areas. These areas were defined based on the actual position of each fin in the real fish.

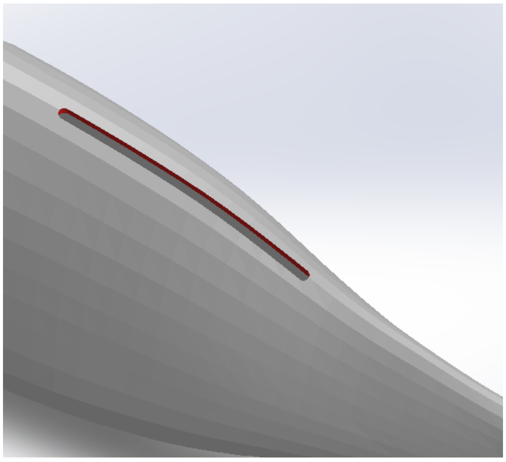

Figure 2.12: Slotted hole for the dorsal fin.

2.2.1 Body-sensor connection system

In order to carry out the experiments, it was also necessary to design a connection system with the sensor that would also allow the fins to be powered. The system developed consists of three components: a hollow threaded rod, and two specially designed parts (3D printed). The first, through the rod, is connected to the body of the fish, while, the second, through three simple screws, is connected to the sensor. Finally, another three screws connect the two parts described above, thus creating a firm connection between sensor and fish. Furthermore, when fully assembled, there is a cavity between the parts and the one connected to the fish has an opening. In this way, the supply wires are able to come out from the body of the robot through the rod, the cavity and the opening; without interfering with the assembly and minimising interference with the fluid dynamics of the model.

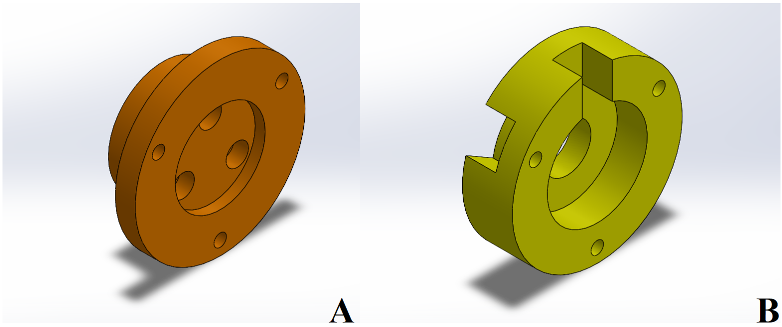

Figure 2.13: In figure A (orange) is shown the part that is connected to the sensor while in figure B (yellow) is shown the part that is connected to the fish through the rod.

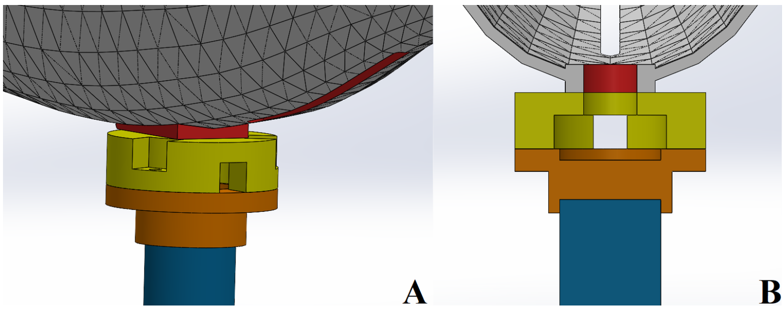

Figure 2.14: Figure A shows the whole system, the blue cylinder represents the sensor. Picture B shows a cross section in which can be seen the hole for inserting the hollow threaded rod and the cavity which allows the wires to pass through the system.

The reason why the system was designed in this way is mainly related to the limitations of 3D printing, this multi-part solution drastically reduced the need for supports and the printing time, thus improved the final quality of the model.

In order to locate the point where the hole that allows the rod to be inserted into the body should be positioned, an initial complete prototype (with fins) was built and the vertical passing through the centre of mass of this model was experimentally identified. Based on this measurement, the hole was then positioned and the adjacent structure was thickened to prevent breakage. Furthermore, the centre of mass of the model was located using Solidworks in order to verify the experimental result.

Figure 2.15: Cross-sectional view showing the reinforced area and the hole.

2.3 Fins control

Fins can perform movements thanks to the SMA wires inside them (further information can be found in the state of the art section 1.3.1 and paragraph 2.1).

In order to control these movements, it is necessary to be able to control the temperature of the SMA wires. The raising of this temperature is generated by a current flow through the SMA wire, while the cooling by dissipation. The fins are in fact immersed in water, so cooling is very rapid when the current flow is stopped.

Based on this principle, therefore, to control the movement of the fins it is necessary to control the current flow through the SMA wires. This flow is proportional to the potential difference applied to the ends of the wire, so the control of the fins is done by controlling the voltage applied to the SMA wires.

The control system was therefore required to have two fundamental characteristics:

1 being able to generate variable voltages based on digital inputs;

2 being able to measure the actual current through the SMA wires.

The second feature is necessary in order to control fin movements and also to prevent wire breakage. In fact, SMA wires can burn and lose their properties when heated to high temperatures. The system designed includes the following components:

Component	Function	Quantity	Data-sheet
Teensy 4.0	Controller	1	Teensy 4.0-Specification
ADS1115	Analog-to-Digital Converter	1	ADS1115-PDF
MAX14870	Driver	4	MAX14870-Specification

Table 2.2: Fins control system used components.

The basic idea is to generate high-frequency PWM signals through the Teensy. These PWMs are sent to the drivers, which generate theo utputs that are used to power the SMA wires inside the fins. The duty cycle of the PWM makes it possible to control the actual voltage that the SMA wire sees. Furthermore, the same drivers are also used to measure the current actually flowing through the SMA wires.

This measurement is obtained indirectly through the voltage present across the RSENSE resistor, which is used to limit the current in the driver (see the component's datasheet for further references); this voltage is sent to the Teensy through the analog-to-digital converter. By means of this value (proportional the current one), it is then possible to decide when to stop the PWM signal and thus stop the movement of the fin.

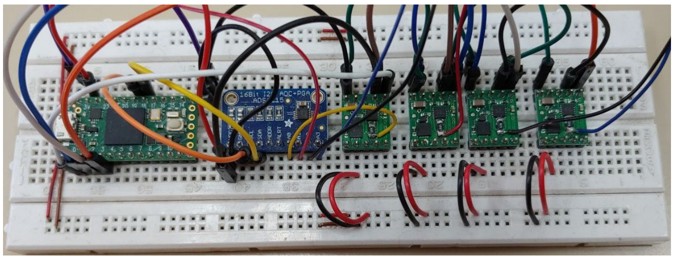

Figure 2.16: Real implementation of the cotrol system.

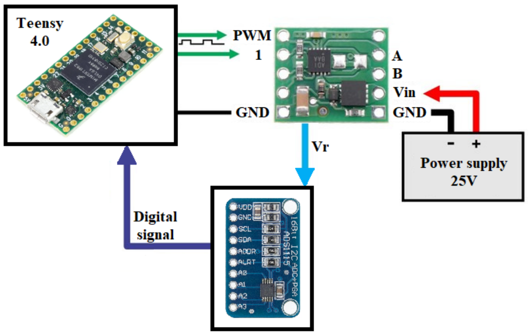

Figure 2.17: Schematic diagram of the implemented system. Points A and B represent the pins to which the ends of the SMA wire should be connected. The output signal from the Teensy indicated with 1 is used because the driver is originally designed to control motors, so, that value is originally needed to indicate the direction in which the motor should turn. In our case it is not necessary so it is maintained at logical 1. "Vr" indicates the voltage used as a reference to calculate the current through the SMA wire.

Through this system, it is therefore possible to control the two characteristic parameters of fins movement:

1 the speed at which the fins move, in fact, higher duty cycles correspond to faster heating of the SMA wires and thus faster movement;

2 the angle at which the fin bends, in fact, by limiting the current it is possible to modulate the amplitudes of movement.

Thanks to the system, up to 4 SMA wires can be controlled at the same time.

2.4 Complete fish setup

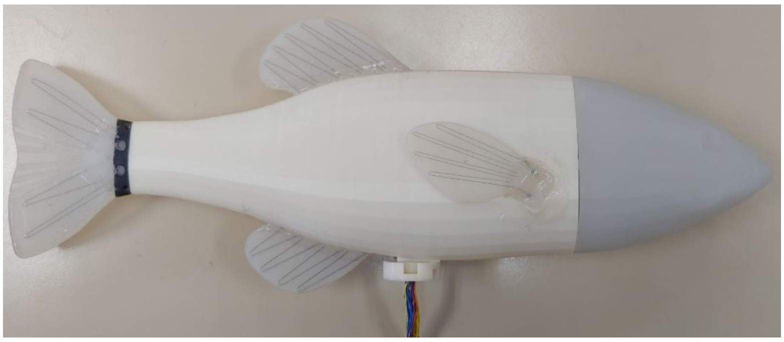

Figure 2.18: Final result of the model realised.

In order to assemble the fish, two pectoral fins, a dorsal fin, an anal fin and a caudal fin were made. All fins were fixed to the body of the fish by means of the same silicone used to make them, with the exception of the caudal fin, which has a rigid plastic base and was glued on with cyanoacrylate.

The overall length of the fish is 460 mm, its maximum thickness 85 mm and its maximum height 170 mm, if we consider only the body without fins the length drops to 382 mm, the height to 125 mm and the thickness 79 mm .

To sustain the model, a support was made using aluminium profiles. To connect this support to the fish-sensor system, a resin connecting clamp was specially designed and manufactured.

Figure 2.19: Final result of the model and the support.

Some features of the model visible in figure 2.19 are commented on below:

- The head and tail joints were covered with insulating tape to prevent unwanted liquid flow.

- There are holes on the top of the structure to allow water to flow and drain away. In fact, the body of the model should be full of water during measurements, so it was necessary to make openings so that water could penetrate during immersion.

- In order to be able to connect the wires to the power source, soldering had to be performed to increase the length of the wires coming out of the fins. To ensure that the welds were watertight, each weld was coated with a heat-shrink sleeve, then the wires were dipped in two-component epoxy resin, and finally everything was covered with insulating tape.

Chapter 3

Materials and methods

The experimental platform is composed of:

- the fins control system (described in section 2.3);
- the fish model realised for the measurements (described in section 2.4);
- an ATI F/T Nano 17 IP 68 sensor with the required electronics (refer to section 3.2 for more information about the signal conditioning circuit);
- an Arduino Uno for the reading of the measurements;
- an aquarium of dimensions 1000x330x400 mm;
- a computer for the communication with the Teensy 4.0 and the Arduino Uno.

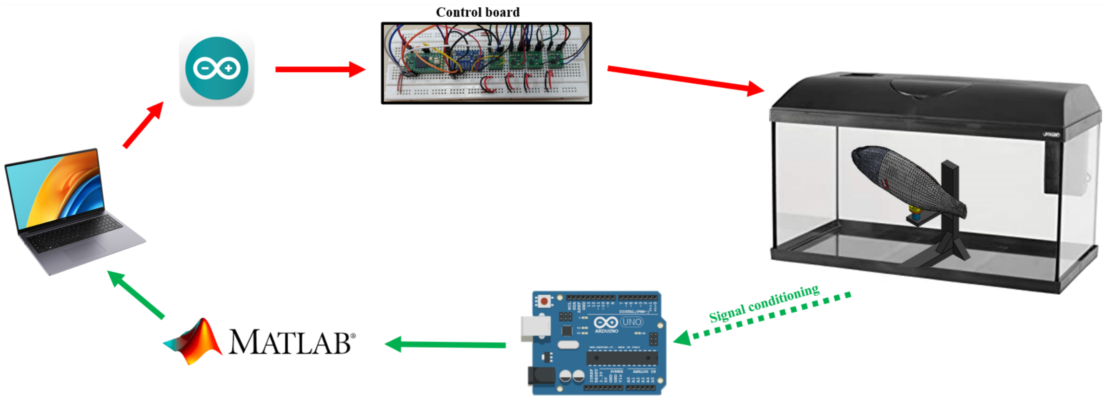

Figure 3.1: Schematic of the experimental platform.

3.1 Features of the ATI Nano 17

The main features of this sensor are its small size, its waterproofness and the excellent performances in terms of resolution and measuring range.

	Fx,Fy	Fz	Tx,Ty	Tz
Sensing Ranges	12 N	17 N	120 Nmm	120 Nmm
Resolution	1/320 N	1/320 N	1/64 Nmm	1/64 Nmm

Table 3.1: Resolution and measuring range. Data obtained from the official page, the calibration performed on the sensor is the SI-12-0.12.

Conversion of output signals to force and torque measurements

The sensor is provided with a 6x6 calibration matrix, this matrix allows the interpretation of the voltages generated by the sensor. These voltages are 6 analogue measurements ($\pm$10V) which do not directly correspond to the force and torque measurements on the various axes (for example, voltage_1 $\neq$ Fx, voltage_2 $\neq$ Fy etc.). In order to obtain the measurements, it is necessary to convert the voltages through the calibration matrix. Before the conversion can be carried out, however, it is necessary to obtain the vector of measurements net of bias. So, for each measurement, it is necessary to calculate the bias vector, then subtract it from the obtained voltages and finally multiply this vector by the calibration matrix. Reference can be made to the process schematised in figure 3.2.

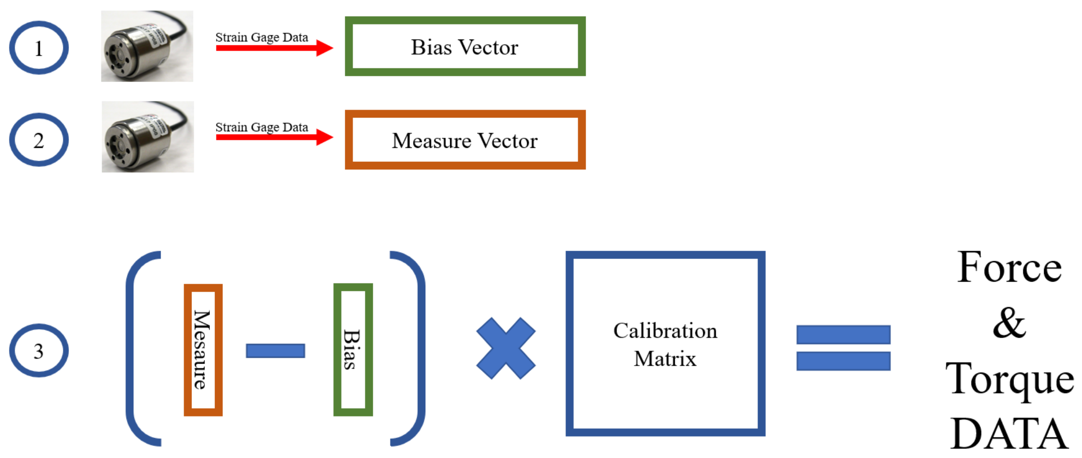

Figure 3.2: Signal conversion process.

3.2 Signal conditioning

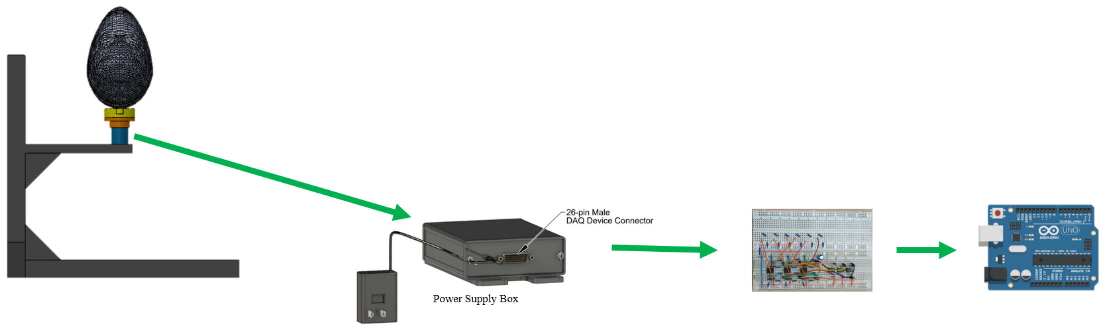

Figure 3.3: Schematic of the signal flow from the sensor to the Arduino Uno.

The reading of output voltages from the sensor is done through a common Arduino Uno. This component, however, can only read signals between 0 and 5 V, while the range of possible sensor output values varies between -10 and 10 V. In order to make the connection possible, it was designed and constructed a circuit that modifies the output signal from the sensor.

First of all, the range actually used during the experiments was assessed and after numerous measurements it was found that the values obtained were all within the ± 2.5 V range. Therefore, in order to improve the quality of the results by decreasing the signal compression required for reading, and considering a large safety margin, it was designed a circuit that could convert signals between ± 5 V to signals between 0 and 5 V so that reading through the Arduino Uno would be possible.

This circuit is based on the use of operational amplifiers (OPAMP), in particular it is composed of three fundamental sections:

1 decoupling stage. The output signal from the sensor's power supply system is decoupled from the downstream electronics so that the signal does not be affected;

2 summing stage. A 5 V offset is added to the decoupled signal in order to convert the ± 5 V range into a 0-10 V range;

3 compression stage. The signal between 0 and 10 V is divided by two via voltage dividers so that the range is changed to 0-5 V, which was the desired goal.

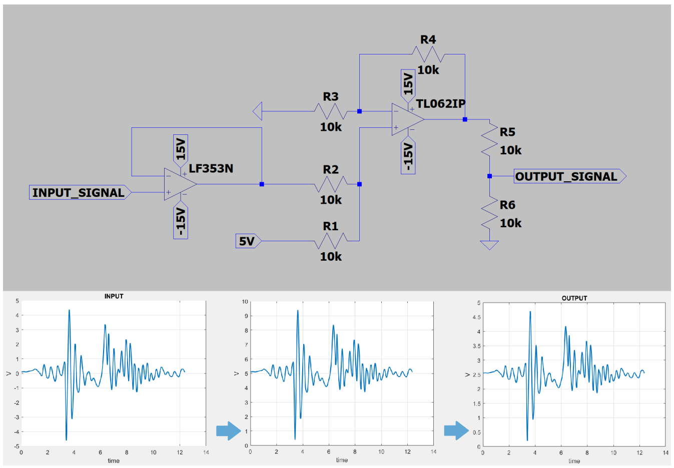

Figure 3.4: Schematic of the circuit designed for a single channel. Graphs are matched with the three sections of the circuit to illustrate how an ideal signal varies during its flow through the various stages.

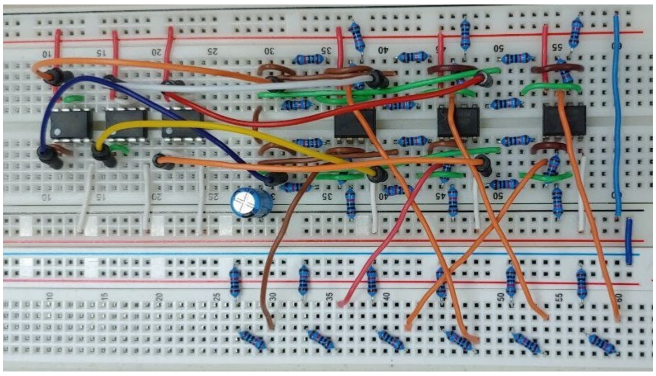

Figure 3.5: Real implementation of the complete circuit.

In the following table the components used to build the circuit are listed.

Component	Number	Data-sheet
TI LF353-N	3	LF353N-PDF
TI TL062IP	3	TL062IP-PDF
10K resistors 1%	36	-

Table 3.2: Components used in the signal conditioning circuit.

3.2.1 Performance of the system

To evaluate the performance of the system composed by the circuit described in section 3.2 and the Arduino Uno board, the following test was carried out.

Instead of using the sensor output signals as input, a voltage generator was connected to the six channels of the circuit simultaneously. Subsequently, the generator values were varied between ±5 V and measurements were taken. The values actually measured were then compared with the theoretical values that should have been measured in the absence of errors.

To perform the comparison between theoretical and actual value, 15-second measurements were taken, and the average of this period was taken as the value actually measured. The points obtained in this way were used to derive straight lines, for each channel. The coefficients of these lines were obtained using Matlab's polyfit command, that computes the coefficients of the polynomial that is a best fit (in a least-squares sense) for the data. These lines were then plotted on diagrams with the actual measured values on the ordinate and the theoretical values on the abscissa. In the ideal case, the straight lines should have been the bisectors of the first quadrant, but being in a real case, a deviation can be seen. Were considered 67 points, with an higher density in the range ±2 V, that is the range into which most of the measurements obtained during the experiments were located. The results obtained are shown below.

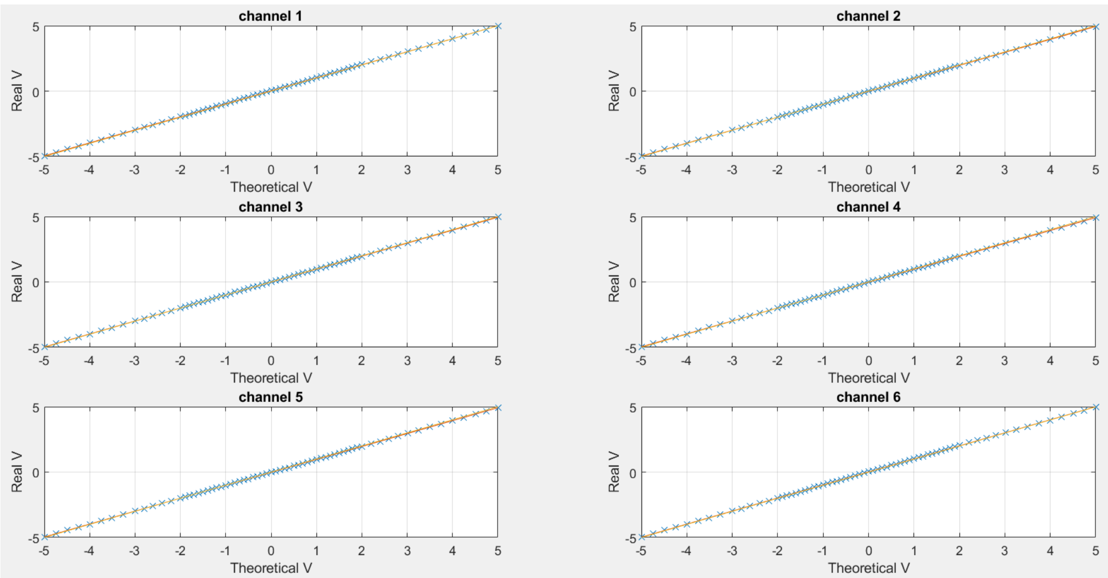

Figure 3.6: The image shows the calculated line in red, the ideal line in yellow, and the points taken into account in the measurements in blue.

As can be seen in figure 3.6, the lines are practically overlapping, which demonstrates the small entity of the error. By numerically evaluating the error (in absolute terms) as the distance between the two lines over 1000 equally-spaced points, for each channel, the average error is between 0.025 and 0.035, while the maximum one is between 0.05 and 0.07.

3.3 Alternative interface between computer and sensor

An interface was also developed in Labview. To develop this interface instead of the Arduino Uno board, a CompactRio 9030 equipped with the NI9381 and NI9215 expansion modules was used. The NI9381 module basically performs the same function as the Arduino, allowing readings between 0-5 V. For the connection between the CompactRio and the breadboard was used a cable with a 37-pin connector appropriately adapted.

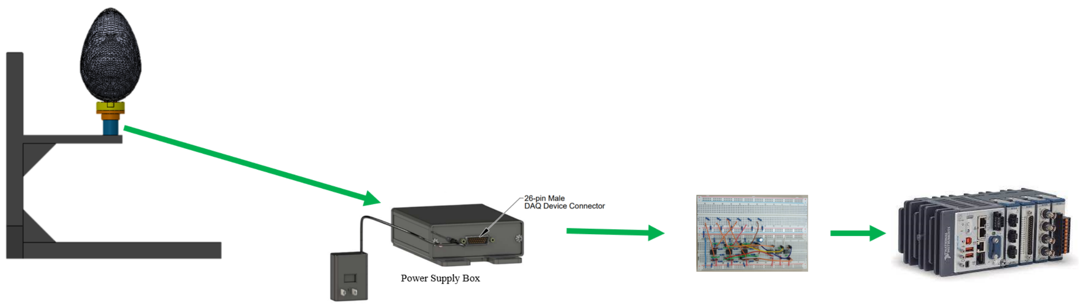

Figure 3.7: Schematic of the signal flow from the sensor to the CompactRio.

In this version, since more analogue inputs are available, in addition to the six output voltages from the sensor (read through the NI9381 module), the actual value of the 5 V offset signal, which is used in the circuit described in section 3.2, is also read.

This signal is read through the NI9215 module, which can read values between ±10 V, so there are no saturation problems (it was not possible to use this module to directly read the sensor output signals because it has only four analogue inputs).

By actually reading the offset value, it was expected to improve the accuracy of the readings compared to the version implemented with Arduino Uno, which treats this value as absolute number and processes it through software. In the Arduino-based system, in fact, this reading is impossible because the board has only six analogue input ports. Anyway, it would also be useless because the oscillations above 5 V would be saturated.

The interface developed in Labview based on the above-mentioned hardware thus makes it possible to display, in real time, forces, torques and the actual value of the offset voltage. It is also possible to manage the basic data acquisition parameters via the graphic interface.

However, after some comparisons between the measurements obtained through the Arduino board and those obtained through the CompactRio, it was highlighted that the noise was greater in the second solution. The reason is probably due to the connection between the NI9381 module and the signal conditioning circuit; unfortunately, as the circuit was necessary for the purpose of the measurements, it was not possible to overcome this problem. For this reason, the solution using the Arduino Uno board was chosen.

Figure 3.8: HMI developed in Labview.

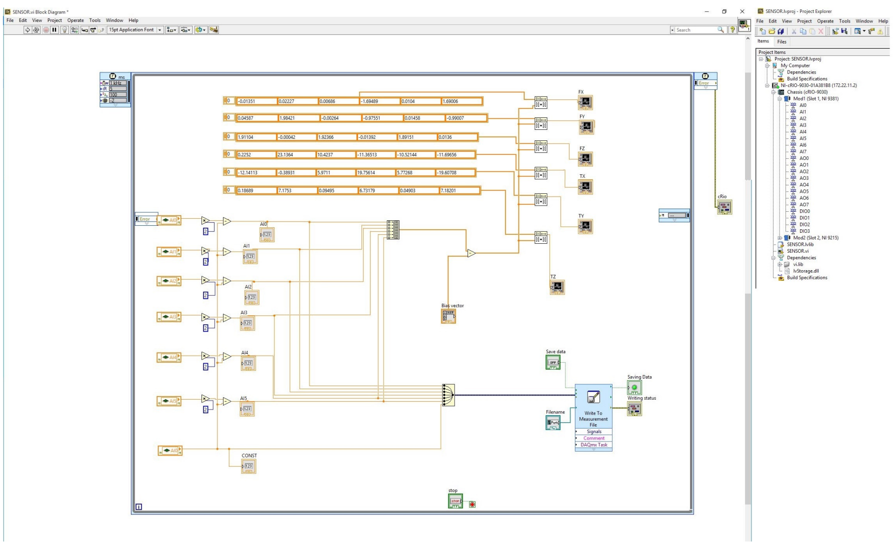

Figure 3.9: Software developed in Labview.

3.4 Software Developed

3.4.1 Teensy 4.0

The control software for the Teensy board was developed directly through the Arduino IDE, since the board used was one of the supported ones. A code for calibrating the fins and one for actually carrying out the experiments were developed. The code for the calibration (refer to the 3.5.2 section for more information on this process) allows to:

- select which SMA wire has to be supplied, (due to the implemented hardware, up to four SMA wires can be connected at the same time);
- select the PWM duty cycle;
- select the PWM duration time;
- read the value of the amount of current circulating in the SMA wire.

Through an interface implemented directly in the serial plotter, the code prompts to select the three parameters, once they are selected it performs the test and prints the values of the current. Finally, it gives the possibility to select new parameters to perform other measurements or exit the execution. In addition, to prevent unwanted operation, if the parameters entered are outside the possible ranges, the programme returns error messages and blocks execution. This code made it possible to drastically speed up calibration operations that otherwise would have had to be carried out manually by directly controlling the current generator.

Unfortunately, it was not possible to generate a code for the execution of fins movements that would work automatically through an interface, because in addition to the large amounts of data generated by the calibrations, which would have had to be handled automatically, it would have been necessary to request dozens of parameters at each execution, thus making the code writing process very long and complex. A malfunction would also have risked burning out the fins and thus delaying the measurements for days. It was therefore decided to write a code in a modular way, with each module allowing a particular function to be performed, and depending on the needs of the test, the various modules were then assembled in sequence. The main features of the modules are:

- movement speed control;
- bending angle limitation based on calibration data;
- movement of several SMA wires (up to 4) simultaneously or sequentially;
- variation of the SMA wires supply signal type (ramp or step);
- possibility of performing repetitions at defined intervals.

3.4.2 Arduino

Also in this case, the code was developed directly in the Arduino IDE. The realised code, once started, reads the voltage values on the analogue pins continuously and sends them thorugh serial communication. The sampling frequency was set at 110Hz.

3.4.3 Matlab

Using Matlab software, the measurements were saved, filtered and processed. The communication with the Arduino Uno was carried out through the serial port. The conversion of voltage measurements to torque measurements was carried out as illustrated in section 3.1.

3.5 Measurement Methodology

3.5.1 Frame of reference

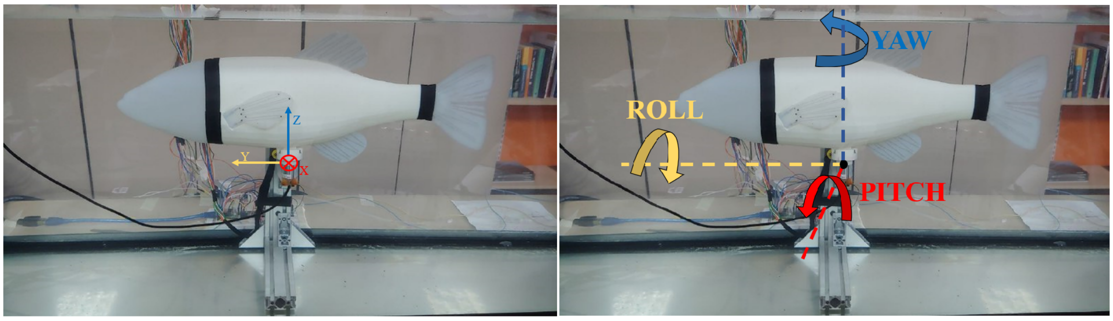

Figure 3.10: Frame of reference of the system.

The measurements were performed with respect to the reference system illustrated in Figure 3.10. The origin of the axes is located at 24 mm from the lower edge of the fish's body on the vertical line passing through the COM. Given the configuration of the axes, we can define the torque along X (Tx) as pitch torque, the one along Y (Ty) as roll torque and the one along Z (Tz) as yaw torque; in the continuation of the document, the two nomenclatures will be used equivalently. During the measurements, the model was not free to move but rigidly bound to the support.

3.5.2 Fins calibration

The different fins (caudal, anal, pectoral, dorsal) differ from each other in size, shape, weight, number and length of the SMA wires. Furthermore, even when evaluating the same types of fins, each one has different characteristics from the others due to the construction process, which, being manual, does not always give exactly the same result. For these reasons, the first step in taking measurements is to calibrate the fins. Thanks to this process, the current limits reached by each SMA wire are tabulated as a function of the different duty cycles of the PWM signals. The duty cycles were selected to limit the maximum current between 900 and 1000 mA. This decision was taken to avert the risk of burning the SMA wires.

The different duty cycles of the PWM signals correspond to different speeds while by limiting the current it is possible to set the different banding angles. Furthermore, the relationship between current and bending angle was assumed to be linear (fixing the applied duty cycle): i.e. if the maximum bending angle corresponds to a current of 100 mA, the current causing a bending equal to an half of the maximum one was assumed to be 50 mA, and so on. This approximation was made on the basis of previous studies [**21**], which confirmed this correlation. These works have also shown that the maximum bending angle of the fins is 40°.

The values were obtained for three different speeds, corresponding to slow medium and fast movements, and three different bending angles, which we define as minimum, medium and maximum. In this way, a 3x3 table of values was obtained for each SMA wire.

3.5.3 Measurements reference

The Teensy and Arduino boards are completely disconnected, so without a reference, it is difficult to find the exact correspondence between inputs, i.e. PWM signals, and outputs, i.e. generated torques. For this reason, in order to avoid misinterpretation of the results, each different configuration was first tested with a physical connection between Teensy and Arduino used as a reference. The connection was made through two digital pins in order to keep track of the time periods in which the PWM signals were generated (i.e. the intervals in which the fins were energised). By superimposing this information on the graphs of the measured torques, it was possible to identify precisely what each measured peak corresponds to.

3.5.4 Test scheduling

In order to avoid interference in the measurements, the tests were carried out with intervals of some minutes between them so that the fins recovered their original temperature, and during each test a recovery time of approximately 3-5 seconds was ensured between one movement and the subsequent one. The amount of recovery time depended on the size of the fin, in order to minimise residual vibrations in the system.

3.5.5 Influence of the slope of the power supply signal

Normally during the tests, the SMA wires were supplied with “actual voltages" that varied sharply from zero to the maximum value and vice versa, thus using signals that could be approximated by square waves. However, this methodology generates an undesirable effect in the measurements: the forward movement of the fin, i.e. the movement from the initial position to the final position, is slower than the return movement, i.e. the movement from the final position to the initial position.

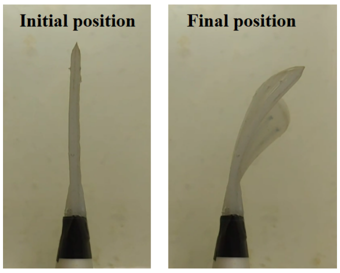

Figure 3.11: Initial and final position of the caudal fin movement.

From the measurement point of view, this phenomenon results in greater torque peaks in the return phase than in the forward phase. To avoid this problem, it has been shown that it is sufficient to use, instead of a supply signal that varies sharply from maximum to zero, one that makes this transition through a ramp. The slope of the ramp allows the magnitude of this phenomenon to be controlled: ramps with steep slopes do not solve the problem, while ramps with poor slopes cause a jerky movement of the fin. In the case of the tests, this result was obtained by gradually varying the duty cycle value from maximum to zero.

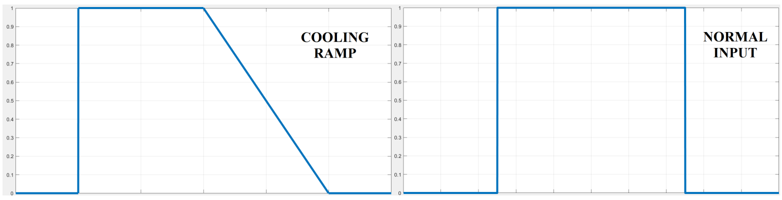

Figure 3.12: Different input signals used to supply the SMA wires.

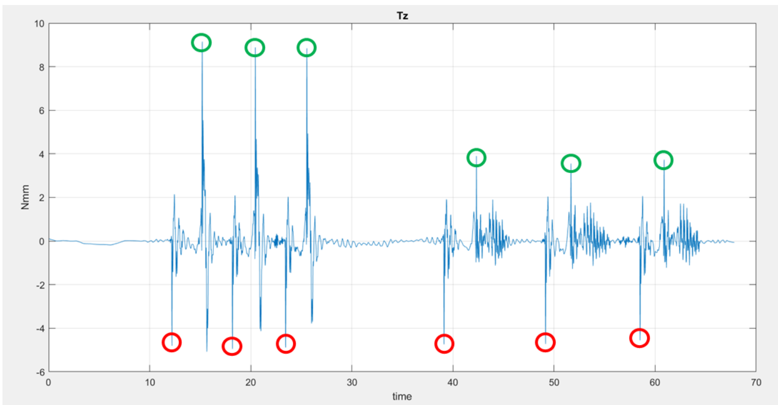

Figure 3.13: Torques generated on the Z axis by performing three movements of the caudal fin at low speed with and without a cooling ramp.

In figure 3.13 we can see the torques measured along Z axis during six movements of the caudal fin performed at low speed. The first three movements are performed with a normal power signal while the others are performed with the cooling ramp.

The peaks of the return phase are highlighted in green while those of the forward phase are highlighted in red. As we can see in all the movements carried out with a cooling ramp, the peaks generated during the return phase are drastically reduced while the ones generated during the forward phase show small variations. However, it should be considered that movements performed with a ramp are significantly slower than the ones generated without it.

In particular, the average of the green peaks without a cooling ramp is 8.80 Nmm while whit it is 3.72 Nmm, this decrease corresponds to a percentage reduction of 57.75%. Instead, the average of the red peaks without the cooling ramp is -4.87 Nmm while whit it is -4.66 Nmm, so the percentage reduction is 4.3%. The reduction in this case is probably due to the longer rest time that the SMA wire has during the movements with cooling ramp.

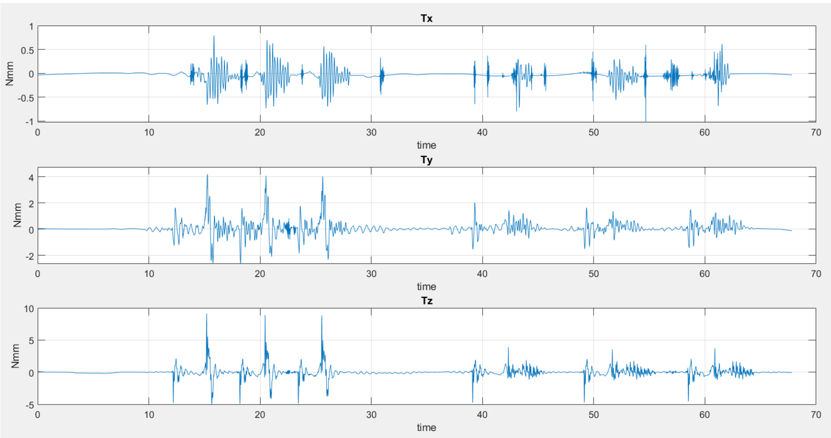

Figure 3.14: Torques generated on the three axes by performing three movements with and without a cooling ramp.

In figure 3.14 we can see the torques generated on the three axes. It is evident that the results on the y-axis are similar to those on the z-axis, while on the x-axis the measurements are not reliable because of the amount of noise present and the small magnitude of the torques.

Anyway, during the tests carried out to measure the torques generated through the various movements, the return phases were not considered, so cooling ramps were not used.

Chapter 4

Experiments results and analysis

In order to evaluate the torques produced by the different movements of the fins, summary tables were produced. Each table proposes the average torque measured, and its standard deviation, as a function of bending angle and speed; refer to section 3.5 for a detailed explanation of the used methodology.

Unfortunately, it was not possible to obtain values for all the movement combinations due to the oscillations and the noise present in the measurements; only measurements with clearly distinguishable peaks were considered.

The tables showing the parameters in terms of maximum current and duty cycle of the PWM, show current ranges that are referred to the measurements obtained for the two SMA wires, left and right side. Also note that the PWM duty cycle has a maximum value of 255, which would correspond to a continuous signal of 25 V.

The actual values of velocity and angle were not measured because the purpose of this work was to generate data for an high-level fuzzy logic style control, anyway they can be estimated based on the previous studies about the individual fins [**21**]. All the values in the torque tables are in Nmm.

4.1 Caudal fin

For each type of movement were performed four repetitions. The selected values correspond to the torque peaks generated during the forward movements, while the return ones have been neglected because they are mainly influenced by the structure of the model. In fact, since the fish is firmly bound to the support, the fins do not stop their movement in a soft manner but with bounces and this phenomenon affects the measurements; see section 3.5.5 for further details.

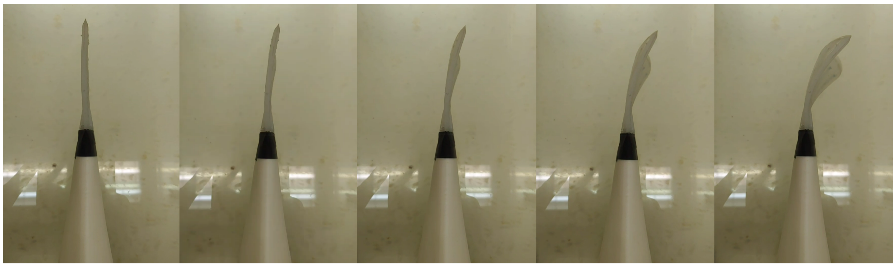

Figure 4.1: Caudal fin leftward movement.

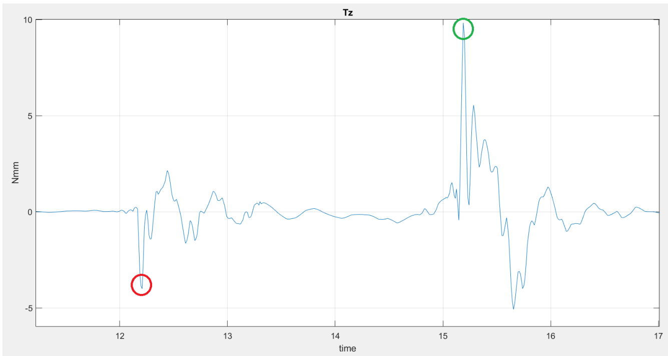

Figure 4.2: Measure of the typical trend of the torque generated by the movement of the caudal fin. It is possible to see the peak generated during the forward movement in red and the one generated during the backward movement in green. The measurement was taken at the lowest possible speed so that the two peaks could be clearly visible and separated.

As we can see in figure 4.2, the typical measurement has two peaks that trigger oscillatory phenomena: one during the forward and one during the backward movement.

Unfortunately, oscillations are inevitable as they are generated by a multitude of factors:

- SMA contraction generates high-frequency vibrations;

- the forces propagate through the hollow structure of the model, which is firmly constrained and therefore tends to resist movement, generating vibrations;
- the movement of the fins in the water generates waves.

The sum of these three factors results in the oscillations visible during the measurements, furthermore, the electrical noise generated in the transmission, conversion and reading of the signal must also be taken into account.

Caudal fin torques relative to the X-axis were not measured during any type of movement. For this reason, no reference to pitch torques is made in this section .

4.1.1 Complete caudal fin

Complete caudal fin movements were carried out with the following parameters:

PWM duty cycle	Maximum current [mA]
200	780-800
225	880-900
255	980-1000

Table 4.1: Caudal fin parameters.

Complete caudal fin - rightward movement

Figure 4.3: Image showing the rightward movement of the caudal fin.

Speed/Angle	Minimum	Medium	Maximum
Slow	-4.92 , s=0.218	-6.46 , s=0.450	-5.43 , s=0.437
Medium	-	-7.18 , s=0.440	-6.20 , s=0.211
Fast	-	-	-6.58 , s=0.494

Table 4.2: Torques [Nmm] generated with different combinations of speed and angle on the Z-axis. Rightward movement of the caudal fin.

Speed/Angle	Minimum	Medium	Maximum
Slow	-2.48 , s=0.246	-2.67 , s=0.305	-2.39 , s=0.233
Medium	-	-3.85 , s=0.690	-3.74 , s=0.980
Fast	-	-	-3.72 , s=0.800

Table 4.3: Torques [Nmm] generated with different combinations of speed and angle on the Y-axis. Rightward movement of the caudal fin.

In table 4.2 we find the torques corresponding to the Z-axis movements, as we can see the maximum value is obtained through the combination of medium angle and medium velocity. The range of the tabulated values is 2.26 Nmm.

In table 4.3 are reported the torques corresponding to the roll movements, the maximum value is obtained again through the combination of medium angle and medium velocity, in this case, however, due to the high standard deviation of the measured values this consideration is unreliable. In fact, peaks greater than 5 Nmm (in modulus) were measured during the tests. In this case, the range of tabulated values is 1.37 Nmm.

Complete caudal fin - leftward movement

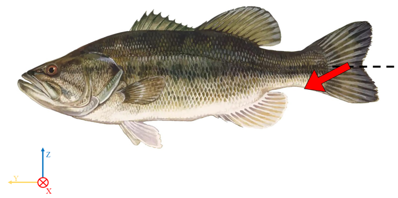

Figure 4.4: Image showing the leftward movement of the caudal fin.

Speed/Angle	Minimum	Medium	Maximum
Slow	5.46 , s=0.093	7.34 , s=0.313	6.00 , s=0.274
Medium	-	8.02 , s=0.327	6.77 , s=0.424
Fast	-	-	7.79 , s=0.263

Table 4.4: Torques [Nmm] generated with different combinations of speed and angle on the Z-axis. Leftward movement of the caudal fin.

Speed/Angle	Minimum	Medium	Maximum
Slow	2.27 , s=0.277	2.68 , s=0.452	2.16 , s=0.372
Medium	-	3.01 , s=0.247	2.96 , s=0.358
Fast	-	-	3.12 , s=0.404

Table 4.5: Torques [Nmm] generated with different combinations of speed and angle on the Y-axis. Leftward movement of the caudal fin.

In table 4.4 are reported the torques corresponding to the yaw movements, as we can see the maximum value is obtained again through the combination of medium angle and medium velocity, in this case the best combination generates an average torque 11.7% higher than the one generated with the same movement on the opposite side. The range of tabulated values is 2.56 Nmm.

In table 4.5 we find the torques corresponding to the roll movements, the maximum value is obtained through the combination of maximum angle and maximum velocity. However, the increment compared to the value obtained through the combination of medium velocity and medium angle, which was the best condition in the previous measurements, is only 3.6%. The range of tabulated values is 0.85 Nmm.

4.1.2 Caudal fin upper part

The movements of the upper part of the caudal fin were carried out with the following parameters:

PWM duty cycle	Maximum current [mA]
90	620-640
110	760-780
130	960-980

Table 4.6: Parameters of the upper part of the caudal fin.

The values of the duty cycles are significantly lower than the previous ones due to the difference in length between the SMA wires.

Caudal fin upper part - rightward movement

Figure 4.5: Image showing the rightward movement of the upper part of the caudal fin.

Speed/Angle	Minimum	Medium	Maximum
Slow	-1.85 , s=0.199	-2.1 , s=0.143	-2.08 , s=0.097
Medium	-	-2.7 , s=0.174	-2.46 , s=0.184
Fast	-	-	-3.01 , s=0.110

Table 4.7: Torques [Nmm] generated with different combinations of speed and angle on the Z-axis. Rightward movement of the upper part of the caudal fin.

In table 4.7 are reported the torques corresponding to the yaw movements, as we can see the maximum value is obtained through the combination of maximum angle and maximum speed. In this case we can see that the standard deviations are significantly lower than those of the previous measurements, highlighting movements characterised by greater repeatability. The range of tabulated values is 1.16 Nmm.

On the other hand, on the Y-axis the oscillations caused by the movements are too high so it is not possible to clearly distinguish the peaks corresponding to the forward motion as a function of the various combinations. A table of roll toruqes was therefore not produced. The only combination that showed distinguishable peaks was the one of maximum angle and velocity, the values obtained are:

average value = -1.68 Nmm   standard deviation = 0.162.

Caudal fin upper part - leftward movement

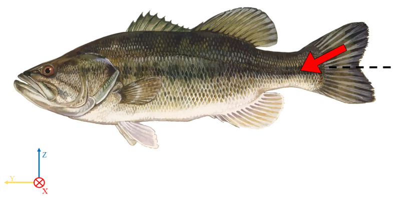

Figure 4.6: Image showing the leftward movement of the upper part of the caudal fin.

Speed/Angle	Minimum	Medium	Maximum
Slow	2.24 , s=0.340	2.86 , s=0.248	2.58 , s=0.232
Medium	-	3.53 , s=0.136	3.20 , s=0.298
Fast	-	-	4.14 , s=0.346

Table 4.8: Torques [Nmm] generated with different combinations of speed and angle on the Z-axis. Leftward movement of the upper part of the caudal fin.

Table 4.8 shows the torques corresponding to the Z-axis movements, as in the previous case, the maximum value is obtained through the combination of maximum angle and maximum speed. In particular, the increment in absolute terms of the generated torque is 37.5% with respect to the rightward case. It is necessary to point out that, in this case, the standard deviations are also higher. The range of tabulated values is 1.9 Nmm.

In relation to the torques on the Y-axis, we find the same phenomenon highlighted with the rightward movement. The values obtained with maximum angle and maximum speed are:

$$\text{average value} = 2.30 \text{ Nmm} \qquad \text{standard deviation} = 0.137.$$

4.1.3 Caudal fin lower part

The movements of the lower part of the caudal fin were carried out with the following parameters:

PWM duty cycle	Maximum current [mA]
90	630-650
110	780-800
130	980-1000

Table 4.9: Parameters of the lower part of the caudal fin.

Caudal fin lower part - rightward movement

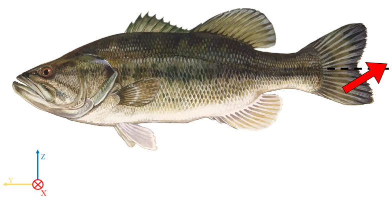

Figure 4.7: Image showing the rightward movement of the lower part of the caudal fin.

Speed/Angle	Minimum	Medium	Maximum
Slow	-2.73 , s=0.349	-3.12 , s=0.363	-2.49 , s=0.149
Medium	-	-3.82 , s=0.188	-3.62 , s=0.138
Fast	-	-	-4.08 , s=0.111

Table 4.10: Torques [Nmm] generated with different combinations of speed and angle on the Z-axis. Rightward movement of the lower part of the caudal fin.

In this case, none of the combinations produced clearly distinguishable peaks in the Y-axis torques. So the results are only reported for the Z-axis torques.

In table 4.10 are shown the measured torques: the maximum value is obtained through the combination of maximum angle and maximum speed. The range of tabulated values is 1.35 Nmm.

Caudal fin lower part - leftward movement

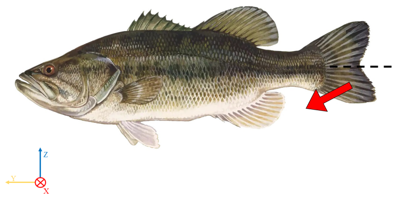

Figure 4.8: Image showing the leftward movement of the lower part of the caudal fin.

Speed/Angle	Minimum	Medium	Maximum
Slow	3.34 , s=0.267	3.60 , s=0.087	3.28 , s=0.238
Medium	-	4.99 , s=0.417	4.08 , s=0.206
Fast	-	-	5.50 , s=0.293

Table 4.11: Torques [Nmm] generated with different combinations of speed and angle on the Z-axis. Leftward movement of the lower part of the caudal fin.

In table 4.11 are reported the torques corresponding to the yaw movements, as in the previous case, the maximum value is obtained through the combination of maximum angle and maximum speed. In particular, the increment in absolute terms of the generated torque is 34.8% with respect to the rightward case. The range of tabulated values is 2.16 Nmm.

In this case, in contrast to the previous one, it was possible to evaluate the roll torque generated with the combination of maximum speed and maximum angle, the results are:

$$\text{average value} = 1.77 \text{ Nmm} \qquad \text{standard deviation} = 0.259.$$

4.1.4 Resume of the results about the caudal fin

Movement	Best Combination (BC)	BC torque value	Range
Complete-right	Med angle-Med Speed	-7.18 Nmm , s=0.440	2.26 Nmm
Complete-left	Med angle-Med Speed	8.02 Nmm , s=0.327	2.56 Nmm
Upper-right	Max angle-Max Speed	-3.01 Nmm, s=0.110	1.16 Nmm
Upper-left	Max angle-Max Speed	4.14 Nmm , s=0.346	1.90 Nmm
Lower-right	Max angle-Max Speed	-4.08 Nmm , s=0.111	1.35 Nmm
Lower-left	Max angle-Max Speed	5.50 Nmm , s=0.346	2.16 Nmm

Table 4.12: Resuming table about the caudal fin results on the Z-axis.

Movement	Best Combination (BC)	BC torque value	Range
Complete-right	Med angle-Med Speed	-3.85 Nmm , s=0.690	1.37 Nmm
Complete-left	Max angle-Max Speed	3.12 Nmm , s=0.404	0.85 Nmm
Upper-right	Max angle-Max Speed	-1.68 Nmm, s=0.162	-
Upper-left	Max angle-Max Speed	2.30 Nmm , s=0.137	-
Lower-right	-	-	-
Lower-left	Max angle-Max Speed	1.77 Nmm , s=0.259	-

Table 4.13: Resuming table about the caudal fin results on the Y-axis.

As we can see in the summary tables, the results highlight, in most cases, as the best combination, the one characterized by maximum angle and maximum speed. However, although the measurements are incomplete, they show that at fixed angle the torque increases as the speed increases, while at fixed speed the angle with which the best performance is obtained is the medium angle. Therefore, as we do not have complete data, we cannot conclude that the most frequent combination is the best overall because the torque generated at maximum speed and average angle would have to be evaluated. As shown in the previous studies [**21**] in fact, there is a limit angle beyond which the torques generated during movements decrease.

By evaluating the values of the torques with respect to the Z axis, we can see that movements to the left side produce greater results in modulus than movements to the right. Unfortunately, however, again due to incomplete data, we cannot draw any firm conclusion. This phenomenon could in fact be caused by alignment errors in the assembly or asymmetries in the movement of the fin. In fact, if we evaluate the torques generated by the complete movement of the fin on the Y axis, we notice that in this case the greatest torque is the one generated during the rightward movement, so the notable difference on the individual components could actually be very small if we had the possibility to calculate the resultant torque.

Furthermore, also differences in velocity between the two sides could influence the results. As we note from the measurements, in fact, an increase in speed causes an increase in force, but we are talking about significant increases: in general, the time required by a fast movement is less than an half of the one required by a slow movement. It's true that even with the same supply signal small differences in speed are generated between the two sides of the fin, but they cannot be the only cause of the net variations between the left and right sides, precisely for their magnitude. The significant difference between the two sides is, therefore, probably due to a combination of the above-mentioned factors

For the control purposes the results are quite disappointing , because these measurements are incomplete and, in addition, some of them show too high standard deviations. Finally, an analysis of the ranges (i.e. the difference in modulus between the value measured with the best and worst combination) shows that in some cases the values are quite small, thus not giving much possibility to vary the parameters.

4.2 Dorsal fin

The movements of the dorsal fin were carried out with the parameters reported in table 4.14.

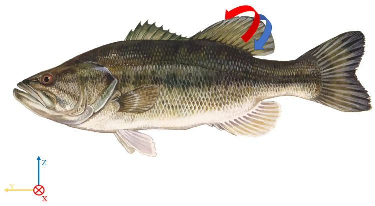

Figure 4.9: Image showing the movements of the dorsal fin. The rightward one is highlighted in red while the leftward one in blue.

PWM duty cycle	Max current [mA]
160	670-690
190	800-820
220	960-980

Table 4.14: Parameters of the dorsal fin.

The measurements for the dorsal fin, as visible in the figure below, are unfortunately excessively affected by oscillations. We cannot therefore distinguish, as for the caudal fin, a peak relative to the forward phase. In this case, then, the RMS value was estimated during the entire movement from the initial position to the final position, again neglecting the return movement. During the tests no torques were measured along the X-axis.

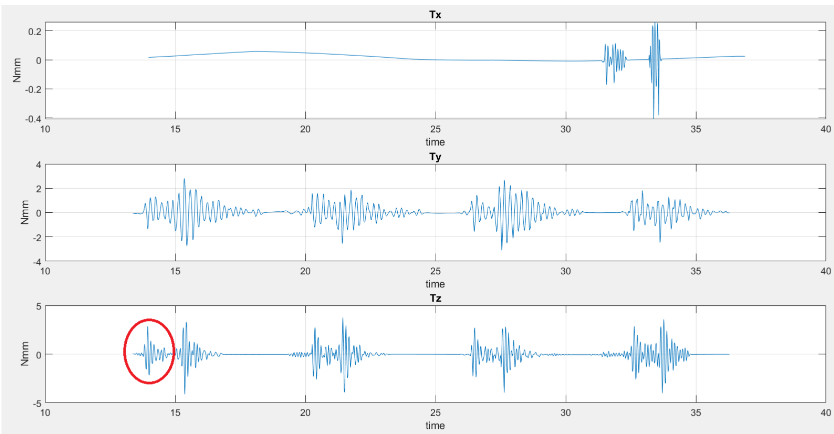

Figure 4.10: Image showing the typical result of the torques generated by the dorsal fin. The red circle highlights the forward movement.

Unfortunately, the angle limitation generates strong vibrations in the structure which could not be avoided. The use of ramps to dampen this effect would have slowed down the movement too much and thus considerably reduced the measured values. For this reason just the maximum angle was considered.

	Min speed	Med speed	Max speed
Tz	0.685 , s=0.036	0.867 , s=0.050	1.271 , s=0.070
Ty	0.460 , s=0.037	0.634 , s=0.070	0.947 , s=0.129

Table 4.15: Torques [RMS-Nmm] generated generated at different speed. Rightward movement of the dorsal fin.

	Min speed	Med speed	Max speed
Tz	0.708 , s=0.035	0.903 , s=0.067	1.306 , s=0.058
Ty	0.429 , s=0.084	0.655 , s=0.042	1.503 , s=0.707

Table 4.16: Torques [RMS-Nmm] generated at different speed. Leftward movement of the dorsal fin.

In the tables are reported Tz and Ty at different speeds and maximum angle, for the leftward movement and for the rightward one. The RMS value considered is the average over the four measurements with its relative standard deviation.

The values measured are quite low but, considering the difference in dimension in comparison to the caudal fin, they are consistent. Furthermore, the proportion between the values obtained for the torques in Ty and Tz is interesting because the distinction is not as pronounced as the one highlighted in the case of the caudal fin. For example, in the rightward movement, the maximum torque in Tz is only 34% greater than the one in Ty. This result is consistent with the positioning of the fin and its function, as it is mainly used to perform Roll movements. Between the measurements taken on the right and left side there are no major variations to be noted except for the Ty generated at maximum speed in the leftward movement. In this case, the value is associated with a high standard deviation and is therefore unreliable. Unfortunately, if we again analyse the results from the perspective of control, they are certainly not satisfactory as they provide only sketchy information. For example, it is not even possible to assess the direction of these pairs.

4.3 Anal fin

The movements of the anal fin were carried out with the parameters reported in table 4.17.

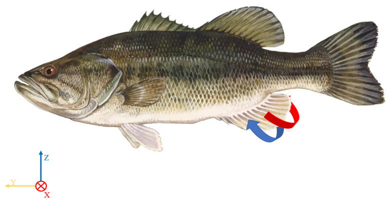

Figure 4.11: Image showing the movements of the anal fin. The rightward one is highlighted in red while the leftward one in blue.

PWM duty cycle	Max current [mA]
80	790-810
100	900-920
120	980-1000

Table 4.17: Parameters of the anal fin.

In the case of the anal fin, the results are very poor, probably due to its proximity to the sensor. Despite numerous attempts, it was not possible to obtain clear measurements in relation to the variation of the parameters (angle and speed) due to the vibrations generated during movement. For this reasons, although the fin produce torques, no measurements are proposed due to the unreliability of the results.

4.4 Combined movements

The objective of the proposed tables was to obtain a database to be used for fish control purposes. In fact, thanks to the data on the torques, it would be possible to deduce the rotations that the model would have made if it had not been constrained, and then based on these results generate combinations of movements such that a desired rotations would have been made. Although the results were not satisfactory, in order to assess whether it was actually possible to coordinate the movement of different fins to achieve a precise result, several movement combinations were tried. Obviously, the combined movement of several fins increases the vibration problems of the model and therefore makes it very difficult to take measurements. However, to perform a conceptual test of the feasibility of this control strategy, the Z-axis torques were evaluated, because they are the ones with the greatest modulus and the available data about this torque is the most complete. First, an S-shaped movement was generated by moving the upper and lower parts of the caudal fin in opposite directions. The best result was achieved by moving the upper part leftward and the lower part rightward. For synchronisation issues, maximum angle and minimum speed were used for both parts. The results are promising because they effectively show a near-torque cancellation during the forward phase. This result was to be expected on the basis of previously obtained data. Unfortunately, however, it was not possible to synchronise the return movement, so a torque is generated. Its peak is around -2 Nmm.

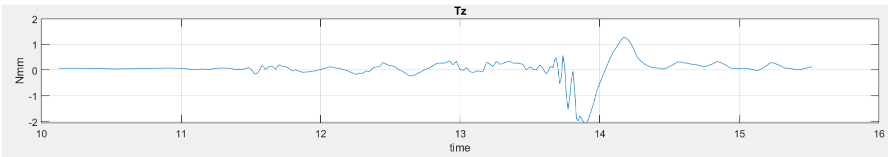

Figure 4.12: Yaw torque generated with the S-shaped movement of the caudal fin.

This result is also very promising because it effectively indicates that it is possible to superimpose the individual measured effects. However, it must be taken into account that in the absence of the constraint, a rotation would have been generated.

The second test was carried out by combining the leftward movement of the caudal fin with the one of the dorsal and anal fins in the opposite direction. In this case, given the different speeds of the respective movements, one slow movement with minimum angle of the caudal fin and two slow movements with maximum angle of the dorsal and anal fins were used. In addition, cooling ramps and recovery times between measurements long enough to minimise residual vibration and thus be able to generate a graph comparable to that of a single caudal fin movement were used. The aim of the test was to check whether there was a reduction in the torque generated in the Z-axis. Unfortunately, it is not possible to identify the same waveform in the measurements for the combined movements as for the single movement.

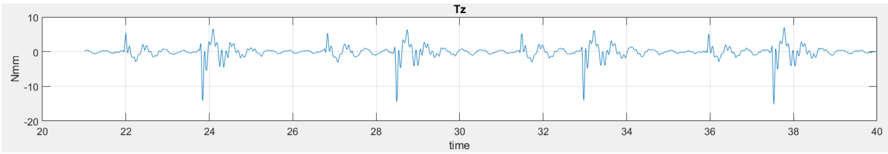

Figure 4.13: Yaw torque generated with the leftward movement of the caudal fin.

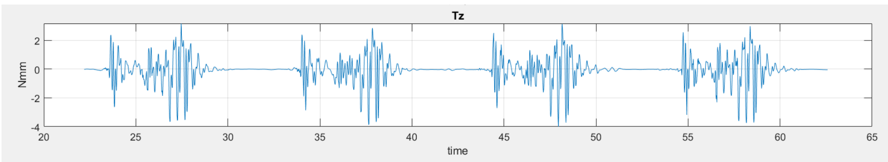

Figure 4.14: Yaw torque generated with the combined movement of the caudal,dorsal and anal fins.

However, in figure 4.14 we can see that the peaks of the oscillations in the forward movement are between 2.8 and -2.8 Nmm, which is significantly below the peaks generated by the single movement; their average value was of 6 Nmm. Furthermore also the torques generated during the return movements seem to be compensating. Again, the result would seem to confirm that the individual effects measured can be superimposed.

Chapter 5

Conclusions and future work

In this work, a 1:1 scale robotic model of largemouth bass was successfully realised. It is characterised by a rigid body and flexible fins actuated through SMA wires and thus without the use of conventional motors.

Subsequently, hardware and software architectures for motion control and data reading were realised with good results and, moreover, a sensor communication interface with an HMI panel was developed through the LabVIEW environment.

Thanks to the realised model, the torques generated by the various movements of the fins were then tabulated with respect to a point of the fish's body belonging to the vertical passing through the centre of mass of the model. Unfortunately, the results are partial, due mainly, to the mechanical noise generated in the structure during the movements. Despite various attempts to reduce this phenomenon, it was not possible to eliminate the problem because it is a characteristic of the model's dynamics. Due to this partiality of the data, the referencing of the measured torques with respect to the centre of mass was unviable; this type of information would have made it possible to calculate most indicative values for the 3D manouevring purposes. However, based on the results obtained and the studies presented in the state of the art, we can state that the order of magnitude of these torques is consistent with other experimental results.

Furthermore, during the tests, it was also evaluated the influence of the rate of change of the duty cycle of the PWM used to control the fins, with respect to the vibrations caused by their motion. It was shown that a gradual variation of this parameter drastically reduces the measured peaks.

Finally, the measurements carried out with respect to the Z-axis by synchronising the movement of several fins, provided results confirming the feasibility of a control strategy based on the superposition of the measured effects with individual movements.

Future work- On the basis of the results obtained, it can therefore be seen that the main limitations encountered with respect to the realisation of a complete database parameterising the effects of fin movements as a function of angle and velocity are the vibrations. They are mainly due to the constraint represented by the sensor, therefore, to overcome this problem, an IMU could be used instead of it. In this way, by mounting the model on a support that leaves it free to rotate with respect to the attachment point, information about the accelerations and angular velocities generated at each movement could be obtained. Thanks to this data it would be possible to realise tables with a similar structure to those proposed in this paper and, subsequently, a control system based on them; again considering the superposition of the individual effects. However, this type of solution would imply the implementation of on-board and waterproof electronic systems.

Appendix A

Base concepts on fish biomechanics

In this section are proposed some basic concepts useful for a better understanding of the document.

A.1 Fins nomenclature and functions

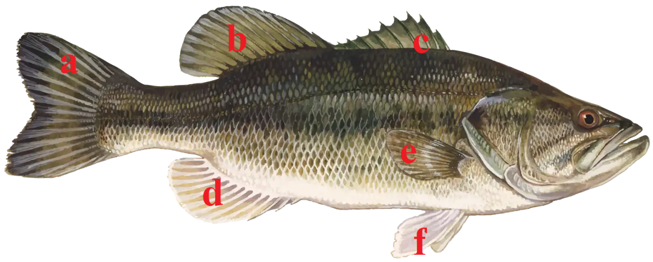

Figure A.1: The fish represented is a largemouth bass (micropterus salmoides). The fins are named as follows: a-caudal fin, b-dorsal fin, c-spiny dorsal fin, d-anal fin, e-pectoral fins(paired fins), f-pelvic fins(paired fins).

Figure A.1 shows the standard nomenclature used to identify the different fins in fishes. However, it is necessary to point out that fins do not have a clear predefined function with regard to fishes locomotion. The purpose of the movements of each individual fin (propulsion/manoeuvring) depends on the characteristics of the fish considered and also on the speed at which it moves. For example, the bluegill sunfish at low speed can generate thrust with its pectoral fins and manoeuvre with the others, while at high speed it generates thrust mainly with the movement of the caudal fin and the pectoral fins remain mostly attached to the body [**14**]. The boxfish, instead, has a similar behaviour at low speed but at high speed it manly generates thrust with synchronous oscillations of the dorsal and anal fins [**16**].

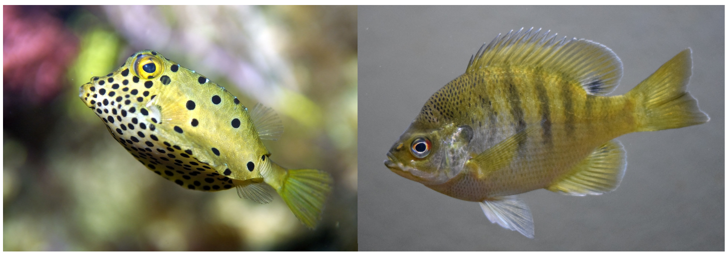

Figure A.2: On the left a specimen of boxfish, on the right a specimen of bluegill sunfish.

Anyway, despite the great variety present in the animal world, we can globally differentiate swimming patterns according to the fins that are predominantly used to generate the fish's propulsion, we distinguish in particular the BCF (Body and/or Caudal Fin propulsion) and the MPF (Medium and/or Paired Fin propulsion). In general, for the purposes of bio-inspired robotics, we can state that the BCF mode is faster, but the MPF mode is more maneuverable [**11**]. Furthermore, BCF mode has simpler dynamics model than the MPF one [**15**].

A.2 Centre Of Mass and Centre Of Buoyancy

Another key aspect in fishes biomechanics are the positions of the COM (centre of mass) and the COB (centre of buoyancy).

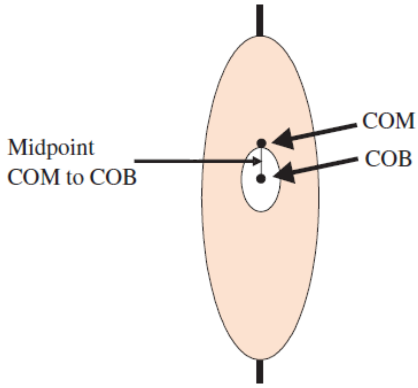

Figure A.3: Typical positions of the COM and the COB. Image taken from E. M. Standen and G. V. Lauder's document [16]. The white oval in the centre of the fish represents the swim bladder cavity of the animal.

In figure A.3 are proposed the typical positions of the COM and the COB. This configuration is the cause of the fishes instability. In the figure is also highlighted the midpoint between COM and COB which is crucial for the calculation of the theoretical torques generated by the fins: the greater the distance of the fin from the midpoint between the COM and COB, the larger the moment arm for that fin [**16**].

Appendix B

Time planning, budgeting and ethical implications

B.1 Time planning

In order to obtain a time schedule of the work done, first the work breakdown structure (WBS) of the project was made. Six macro-categories related to the work development were highlighted:

- **Planning** phase related to the project documentation and planning;
- **Design** phase related to the design of all the elements needed for the project;
- **Construction** phase related to the practical realization of all the components and the final setup;
- **Coding** phase related to the writing of the various codes needed;
- **Measurements** phase related to the tests made in order to obtain the data presented;
- **Closeout** phase related to the analysis of the data obtained and the writing of the document.

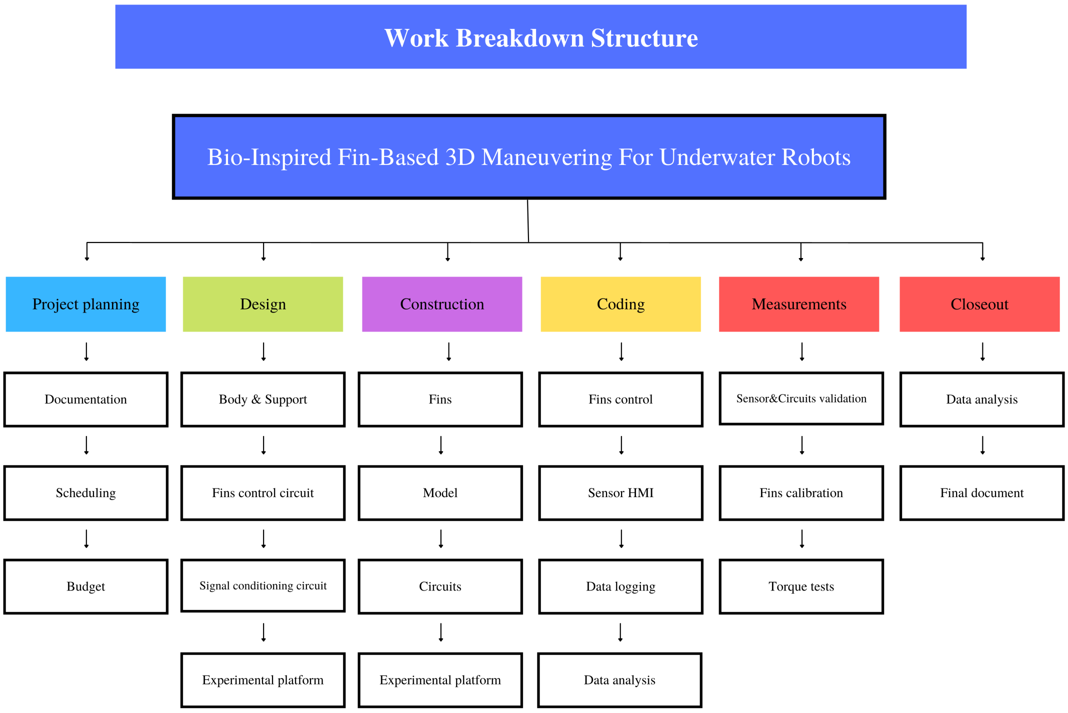

Figure B.1: Work Breakdown Structure

Following the WBS, the time planning of the various activities was carried out. Being a work done independently, in the planning the weekends were not taken into account, although on some occasions the closure of the university impacted the planned progress.

Figure B.2 shows the initial schedule and the one actually achieved, as we can see the main problems were caused by the implementation of the HMI in Labview since initially a learning phase of the platform was required.

1	Activity	Start	Duration	End	Actual start	Actual duration	Actual end
2	Documentation	22/08/2022	10	01/09/2022	22/08/2022	10	01/09/2022
3	Scheduling	30/08/2022	2	01/09/2022	30/08/2022	2	01/09/2022
4	Budget estimation	30/08/2022	2	01/09/2022	30/08/2022	2	01/09/2022
5	Body design	01/09/2022	3	04/09/2022	01/09/2022	3	04/09/2022
6	Support & connection system design	04/09/2022	6	10/09/2022	04/09/2022	5	09/09/2022
7	Fins control circuit design	10/09/2022	7	17/09/2022	09/09/2022	5	14/09/2022
8	Signal conditioning circuit design	17/09/2022	7	24/09/2022	14/09/2022	7	21/09/2022
9	Experimental platform design	24/09/2022	3	27/09/2022	21/09/2022	3	24/09/2022
10	Fins construction	27/09/2022	7	04/10/2022	26/09/2022	7	03/10/2022
11	Model construction	04/10/2022	3	07/10/2022	03/10/2022	2	05/10/2022
12	Circuits construction	27/09/2022	2	29/09/2022	26/09/2022	2	28/09/2022
13	Experimental platform assembly	07/10/2022	2	09/10/2022	05/10/2022	2	07/10/2022
14	Fins control code	09/10/2022	7	16/10/2022	07/10/2022	6	13/10/2022
15	Sensor HMI	16/10/2022	21	06/11/2022	13/10/2022	24	06/11/2022
16	Data logging code	06/11/2022	5	11/11/2022	06/11/2022	5	11/11/2022
17	Data analysis code	11/11/2022	7	18/11/2022	11/11/2022	7	18/11/2022
18	Sensor & circuits validation	18/11/2022	2	20/11/2022	18/11/2022	1	19/11/2022
19	Fins calibration	20/11/2022	6	26/11/2022	21/11/2022	5	26/11/2022
20	Torque tests	26/11/2022	24	20/12/2022	28/11/2022	22	20/12/2022
21		20/12/2022	14	03/01/2023	20/12/2022	14	03/01/2023
22	Data analysis	03/01/2023	14	17/01/2023	03/01/2023	14	17/01/2023
23	Final document	11/01/2023	21	01/02/2023	11/01/2023	21	01/02/2023

On time
1 day in adavance
2 days in adavance
3 days in advance
Delay due to problems
Delay due to weekends

Figure B.2: Initial and final planning, the variations from the schedule are highlighted.

Finally, two GANTT are proposed, the first is related to the initial planning while the second is updated with the actual implementation; the red bar indicates the Christmas break.

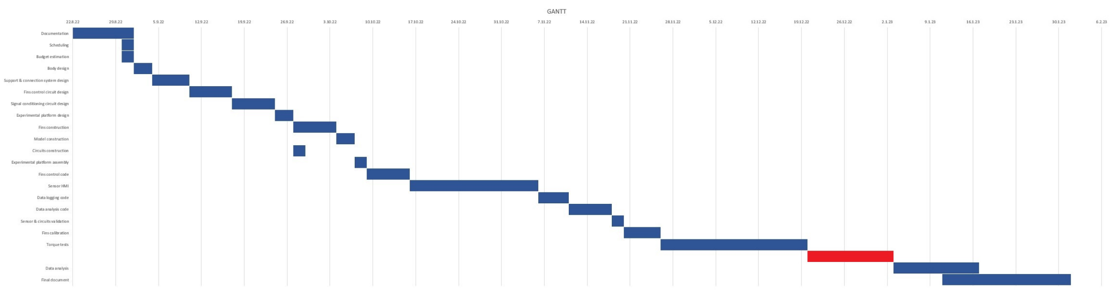

Figure B.3: Starting GANTT

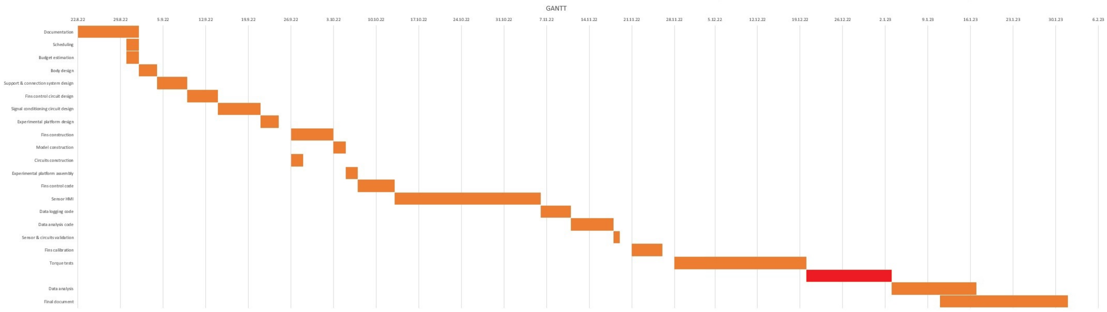

Figure B.4: Actualized GANTT

B.2 Budgeting

This section contains a table with the components needed to realise the project and their cost.

Component	Quantity	Unit price	Total price	Shop
PlatSil Gel 25	900 g	49.61€/900g	49.61 €	Feroca
SMA wires	3 m	6.5€/1m	19,5 €	Musclewires
Teensy 4.0	1	32.44 €	32.44 €	Mouser
Arduino UNO	1	27.6 €	27.6 €	Mouser
ADS1115	2	11.52 €	23.04 €	Amazon
MAX14870	5	13.75 €	68.75 €	Pololu
TI LF353-N	6	1.56 €	9.36 €	Mouser
TI TL062IP	6	0.99 €	5.94 €	Mouser
Resistor 10K	100	0.04 €	4 €	Mouser
Breadboard	2	7.49 €	14.98 €	Mouser
Cables/Screws	/	/	20 €	Common shop
Aluminium profile	1 m	15.78€/1m	15.78 €	R-S
			TOTAL	281 €

Table B.1: Components and prices.

As can be seen, there were included in the budget more components than the ones strictly needed, the reason is manly related to the possible failures, so a safety margin was considered when purchasing components. Some quantities were also determined in relation to the minimum order allowed in the shop. Furthermore, considering the shipping costs, purchasing the exact number of components would have been disadvantageous, because in case of failures as well as the delay in the schedule, the costs would have risen disproportionately.

B.3 Ethical implications

From an ethical point of view, this work has a double significance.

Firstly, the development of robots with characteristics like those of real animals allows to carry out research without risking the mistreatment that is often a problem in this type of study. This would represent a great advance in the field of the research on animal biomechanics.

Secondly, in the specific case of the realised model, the use of submarine robots that can move without using traditional engines could drastically reduce the environmental impact related to research studies on marine environments. Furthermore, this would also apply to all those fields that require underwater operations, such as the maintenance of underwater infrastructure. From this point of view, in fact, the development of this kind of technology would be revolutionary and would open up the field to a series of activities and studies that were unimaginable to date.

In conclusion, we can therefore state that the development of bio-inspired submarine robots actuated by innovative techniques has also important ethical advantages over traditional technologies.

Bibliography

[1] R. Velázquez, C. L. Garzón-Castro, M. Acevedo, M. T. Orvañanos-Guerrero and A. A. Ghavifekr, "Design and Characterization of a Miniature Bio-Inspired Mobile Robot," 2021 12th International Symposium on Advanced Topics in Electrical Engineering (ATEE), 2021, pp. 1-5, doi: 10.1109/ATEE52255.2021.9425096.

[2] A. M. Hoover, S. Burden, Xiao-Yu Fu, S. Shankar Sastry and R. S. Fearing, "Bio-inspired design and dynamic maneuverability of a minimally actuated six-legged robot," 2010 3rd IEEE RAS & EMBS International Conference on Biomedical Robotics and Biomechatronics, 2010, pp. 869-876, doi: 10.1109/BIOROB.2010.5626034.

[3] Z. Yu, Y. Shi, A. Luo, J. Tao and S. X. Yang, "Research on Landing Collision Experiment of Gecko Robot with Bio-inspired Dry Adhesive Foot," 2018 IEEE International Conference on Information and Automation (ICIA), 2018, pp. 336-340, doi: 10.1109/ICInfA.2018.8812558.

[4] S. Ha, S. Thomas, O. Kwon and S. C. Lee, "Bio-inspired robot platform powered by a commercial PEM fuel cell," 2013 13th International Conference on Control, Automation and Systems (ICCAS 2013), 2013, pp. 1703-1707, doi: 10.1109/ICCAS.2013.6704209.

[5] J. -Y. Kim and B. -H. Jun, "Mechanical design of six-legged walking robot, Little Crabster," 2012 Oceans - Yeosu, 2012, pp. 1-8, doi: 10.1109/OCEANS-Yeosu.2012.6263402.

[6] https://spectrum.ieee.org/six-legged-underwater-robot-crabster

[7] Biologically inspired robotics / editors, Yunhui Liu and Dong Sun.p. cm.Includes bibliographical references and index.ISBN 978-1-4398-5488-4 (hardback)1. Robotics. 2. Bionics. 3. Biomimicry. 4. Biomechanics. I. Liu, Yunhui. II. Sun, Dong, 1967- III. Title

[8] Fukuda, Toshio & Chen, Fei & Shi, Qing. (2018). Special Feature on Bio-Inspired Robotics. Applied Sciences. 8. 817. 10.3390/app8050817.

[9] S. Sareh et al., "Bio-inspired tactile sensor sleeve for surgical soft manipulators," 2014 IEEE International Conference on Robotics and Automation (ICRA), 2014, pp. 1454-1459, doi: 10.1109/ICRA.2014.6907043.

[10] Ren Z, Hu K, Wang T, Wen L. Investigation of Fish Caudal Fin Locomotion Using a Bio-Inspired Robotic Model. International Journal of Advanced Robotic Systems. 2016;13(3). doi:10.5772/63571.

[11] J. Li, J. He, y. wang, K. Yu, M. Woźniak and W. Wei, "A Biomimetic Flexible Fishtail Embedded With Shape Memory Alloy Wires," in IEEE Access, vol. 7, pp. 166906-166916, 2019, doi: 10.1109/ACCESS.2019.2953546.

[12] Yang, Y., Xia, Y., Qin, F., Xu, M., Li, W. & Zhang, S. (2016). Development of a bio-inspired transformable robotic fin. Bioinspiration and Biomimetics, 11 (5), 056010-1-056010-12.

[13] P. K. Vidyarthi, K. Mukherjee and B. K. Roy, "Fish-Like Robots And Applications Of Sensor -A Review," 2022 4th International Conference on Energy, Power and Environment (ICEPE), 2022, pp. 1-6, doi: 10.1109/ICEPE55035.2022.9798191.

[14] James Tangorra, Chris Phelan, Chris Esposito, George Lauder, Use of Biorobotic Models of Highly Deformable Fins for Studying the Mechanics and Control of Fin Forces in Fishes, Integrative and Comparative Biology, Volume 51, Issue 1, July 2011, Pages 176–189, https://doi.org/10.1093/icb/icr036

[15] *W. Shao and C. Xu, "Pitch Motion Control of a Soft Bionic Robot Fish Based on Centroid Adjustment," 2019 IEEE International Conference on Mechatronics and Automation (ICMA), 2019, pp. 1883-1888, doi: 10.1109/ICMA.2019.8816287.*

[16] *E. M. Standen, G. V. Lauder; Dorsal and anal fin function in bluegill sunfish Lepomis macrochirus: three-dimensional kinematics during propulsion and maneuvering. J Exp Biol 15 July 2005; 208 (14): 2753–2763. doi: https://doi.org/10.1242/jeb.01706*

[17] *Brinson LC. One-Dimensional Constitutive Behavior of Shape Memory Alloys: Thermomechanical Derivation with Non-Constant Material Functions and Redefined Martensite Internal Variable. Journal of Intelligent Material Systems and Structures. 1993;4(2):229-242. doi:10.1177/1045389X9300400213*

[18] *Christopher J. Esposito, James L. Tangorra, Brooke E. Flammang, George V. Lauder; A robotic fish caudal fin: effects of stiffness and motor program on locomotor performance. J Exp Biol 1 January 2012; 215 (1): 56–67. doi: https://doi.org/10.1242/jeb.062711*

[19] *Coral W, Rossi C, Curet OM, Castro D. Design and assessment of a flexible fish robot actuated by shape memory alloys. Bioinspir Biomim. 2018 Jul 31;13(5):056009. doi: 10.1088/1748-3190/aad0ae. PMID: 29968572.*

[20] *White CH, Lauder GV, Bart-Smith H. Tunabot Flex: a tuna-inspired robot with body flexibility improves high-performance swimming. Bioinspir Biomim. 2021 Mar 5;16(2). doi: 10.1088/1748-3190/abb86d. PMID: 32927442.*

[21] *Coral W, Rossi C. Soft dorsal/anal fins pairs for roll and yaw motion in robotic fish. Bioinspir Biomim. 2022 Nov 23;18(1). doi: 10.1088/1748-3190/aca132. PMID: 36347041.*

[22] *S. Zhang, B. Liu, L. Wang, Q. Yan, K. H. Low and J. Yang, "Design and Implementation of a Lightweight Bioinspired Pectoral Fin Driven by SMA," in IEEE/ASME Transactions on Mechatronics, vol. 19, no. 6, pp. 1773-1785, Dec. 2014, doi: 10.1109/TMECH.2013.2294797.*